Raytheon

PRECIPITABLE WATER

VISIBLE/INFRARED IMAGER/RADIOMETER SUITE ALGORITHM THEORETICAL BASIS DOCUMENT

Version 5: March 2002

H.-L. Huang
H.M. Woolf
Shawn W. Miller
Richard J. Sikorski

RAYTHEON COMPANY
Information Technology and Scientific Services
4400 Forbes Boulevard
Lanham, MD 20706

SRBS Document #: Y3251

EDR: PRECIPITABLE WATER

Doc No: Y3251

Version: 5

Revision: 1

	Function	Name	Signature	Date
Prepared by	EDR Developer	H.-L. HUANG		1/14/02
Approved by	Reviewer	R. SLONAKER		1/30/02
Approved by	Surface Temperature IPT Lead	R. SIKORSKI		2/1/02
Approved by	Chief Scientist	S. MILLER		2/4/02
Released by	Algorithm Lead	P. KEALY		2/5/02

TABLE OF CONTENTS

LIST OF FIGURES

Page

LIST OF TABLES

Page

GLOSSARY OF ACRONYMS

AGI	Advanced Global Imager
AOT	Aerosol Optical Thickness
ATB	Algorithm Theoretical Basis
ATBD	Algorithm Theoretical Basis Document
AVHRR	Advanced Very High Resolution Radiometer
CAMEX	Convection And Moisture EXperiment
COT	Cloud Optical Thickness
DoD	Department of Defense
EDR	Environmental Data Record
EOS	Earth Observing System
FOV	Field of View
GIFOV	Ground Instantaneous Field of View
HC	Horizontal Cell
HCS	Horizontal Cell Size
HRI	Horizontal Reporting Interval
HSR	Horizontal Spatial Resolution
IFOV	Instantaneous Field of View
IP	Intermediate Product
IR	Infrared
LLLS	Low Level Light Sensor
LST	Land Surface Temperature
MAS	MODIS Airborne Simulator
MODIS	Moderate Resolution Imaging Spectroradiometer
NASA	National Aeronautics and Space Administration
nd	No Dimensions
NOAA	National Oceanic and Atmospheric Administration
NPOESS	National Polar-orbiting Operational Environmental Satellite System
NPP	NPOESS Preparatory Program
NAST-I	NPOESS Airborne Sounder Testbed – Interferometer
OLS	Operational Linescan System
PDR	Preliminary Design Review
PLOD	Pressure Layer Optical Depth
PW	Precipitable Water
RDR	Raw Data Record
RMSE	Root Mean Squared Error
RTE	Radiative Transfer Equation
SAFARI	Southern African Regional Science Initiative
SBRS	Santa Barbara Remote Sensing
SDR	Sensor Data Record

SDSM	Solar Diffuser Stability Monitor
SNR	Signal-to-Noise Ratio
SRD	Sensor Requirements Document
SST	Sea Surface Temperature
SUCCESS	SUbsonic Aircraft Contrail and Cloud Effects Special Study
TIROS	Television Infrared Observation Satellite
TOA	Top of Atmosphere
VIIRS	Visible/Infrared Imager/Radiometer Suite
WINCE	WINter Cloud Experiment
WISC-T2000	WIsconsin Snow Cloud - Terra 2000 experiment

ABSTRACT

Precipitable Water is one of more than two dozen Environmental Data Records (EDRs) explicitly required as products to be derived from the Visible/Infrared Imager/Radiometer Suite (VIIRS) sensor slated to fly onboard the National Polar-orbiting Operational Environmental Satellite System (NPOESS), which is scheduled for launch in the late 2000's. The requirements for the VIIRS EDRs are described in detail in the VIIRS Sensor Requirements Document (SRD). These requirements form the foundation from which both the algorithms and the sensor are designed and built. A revised version of the SRD was released in November 1999, detailing a set of new requirements targeted toward the NPOESS Preparatory Program (NPP), a National Aeronautics and Space Administration (NASA) endeavor to build upon the MODIS heritage beginning in 2005. The Precipitable Water (PW) EDR was added to the VIIRS SRD at that time.

The PW EDR will be retrieved globally, both day and night, and under both clear and cloudy conditions. Under cloudy conditions, the retrievals will only include PW above the clouds. This unique baseline algorithm for the PW EDR is a non-linear statistical regression approach similar to the traditional methods for deriving sea surface temperature (SST). Data from five bands will be used in conjunction with solar-viewing geometry and surface pressure to arrive at the final product, which will provide estimates of precipitable water along the line of sight at high spatial resolution to complement the microwave-derived total column product in the NPOESS suite of EDRs.

This document includes a thorough description of the established behavior of the PW EDR. Simulated trade studies, which account for the effects of measurement noise, forward model error, atmospheric state uncertainties, aerosol contamination, and sub-visible cirrus cloud, are documented. VIIRS spectral measurement characteristics related to PW, the historical development of retrieving PW, and a detailed mathematical description of the proposed non-linear "overlap regional" regression retrieval algorithm are also discussed. The simulations have permitted the construction and characterization of a robust package of environmental products which will build upon the existing MODIS heritage.

1.0 INTRODUCTION

1.1 PURPOSE

This Algorithm Theoretical Basis Document (ATBD) describes the algorithms used to retrieve the Precipitable Water (PW) Environmental Data Record (EDR) for VIIRS. The primary purpose of this ATBD is to establish guidelines for the production of the PW EDR. This document will describe the required inputs, the theoretical foundation of the algorithms, the sources and magnitudes of the errors involved, practical considerations for post-launch implementation, and the assumptions and limitations associated with the products.

1.2 SCOPE

This document covers the Algorithm Theoretical Basis (ATB) for operational retrieval of the PW EDR. Any derived products beyond the generation of this EDR will not be discussed.

Section 1 describes the purpose and scope of this document; it also includes a listing of VIIRS documents that will be cited in the following sections. Section 2 provides a brief overview of the motivation for the PW algorithm, including the objectives of the retrievals, the currently designed VIIRS instrument characteristics, and the strategy for retrieval of the PW EDR. Section 3 contains the essence of this document – a complete description of the PW EDR. Consideration is given to the overall structure, the required inputs, a theoretical description of the products, assessment of the error budget, results of ongoing sensitivity studies, practical implementation issues, validation, and the algorithm development schedule. Section 4 provides an overview of the constraints, assumptions and limitations associated with the PW EDR, and Section 5 contains a listing of references cited throughout the course of this document.

1.3 VIIRS DOCUMENTS

Reference to VIIRS documents within this ATBD will be indicated by an italicized number in brackets, e.g., *[V-1]*.

[V-1] VIIRS Surface Type ATBD.

[V-2] VIIRS Aerosol Optical Thickness ATBD.

[V-3] VIIRS Geolocation ATBD.

[V-4] VIIRS Calibration/Validation Plan.

[V-5] VIIRS Cloud Mask ATBD.

[V-6] VIIRS Surface Reflectance ATBD.

1.4 REVISIONS

This is version 5 of this document. It is dated March 2002. There were no versions numbered 1.0 or 2.0; the current version number has been selected to match the delivery of the previously

existing VIIRS EDR ATBDs, which underwent prior version releases. Substantial contributions to prior versions of this document were made by Donglian Sun.

2.0 EXPERIMENT OVERVIEW

2.1 OBJECTIVES OF PW RETRIEVALS

The overall scientific objective of the VIIRS PW EDR is to provide improved, high-spatial-resolution (single VIIRS pixel), global PW fields. PW is defined as the total equivalent water in the line of sight from the top of atmosphere down to the surface (cloud, land, etc.) per unit cross-sectional area. The PW EDR is crucial for our understanding of the hydrological cycle, aerosol-cloud interactions, energy budget, and climate. PW is also an important parameter for deriving other VIIRS EDRs, such as sea surface and land surface temperature. Accurate knowledge about PW will lead to improved SST and LST EDRs, as all the Infrared (IR) VIIRS spectral measurements are strongly affected by water vapor absorption.

2.2 INSTRUMENT CHARACTERISTICS

The VIIRS instrument will now be briefly described to clarify the context of the descriptions of the PW EDR presented in this document. VIIRS can be pictured as a convergence of three existing sensors, two of which have seen extensive operational use at this writing.

The Operational Linescan System (OLS) is the operational visible/infrared scanner for the Department of Defense (DoD). Its unique strengths are controlled growth in spatial resolution through rotation of the Ground Instantaneous Field Of View (GIFOV) and the existence of a Low-Level Light Sensor (LLLS) capable of detecting visible radiation at night. OLS has primarily served as a data source for manual analysis of imagery. The Advanced Very High Resolution Radiometer (AVHRR) is the operational visible/infrared sensor flown on the National Oceanic and Atmospheric Administration (NOAA) Television Infrared Observation Satellite (TIROS-N) series of satellites (Planet, 1988). Its unique strengths are low operational and production cost and the presence of five spectral channels that can be used in a wide number of combinations to produce operational and research products. In December 1999, the National Aeronautics and Space Administration (NASA) launched the Earth Observing System (EOS) morning satellite, *Terra*, which includes the Moderate Resolution Imaging Spectroradiometer (MODIS). This sensor possesses an unprecedented array of 36 spectral bands at resolutions ranging from 250 m to 1 km at nadir, allowing a wide range of satellite-based environmental measurements.

VIIRS will reside on a platform of the NPOESS series of satellites. It is intended to be the product of a convergence between DoD, NOAA and NASA in the form of a single visible/infrared sensor capable of satisfying the needs of all three communities, as well as the research community beyond. As such, VIIRS will require three key attributes: high spatial resolution with controlled growth off nadir, minimal production and operational cost, and a large number of spectral bands to satisfy the requirements for generating accurate operational and scientific products.

Figure 1 illustrates the design concept for VIIRS, designed and built by Raytheon Santa Barbara Remote Sensing (SBRS). At its heart is a rotating telescope scanning mechanism that minimizes the effects of solar impingement and scattered light. Calibration is performed onboard using a solar diffuser for short wavelengths and a V-groove blackbody source and deep space view for

thermal wavelengths. A Solar Diffuser Stability Monitor (SDSM) is also included to track the performance of the solar diffuser. The nominal altitude for NPOESS will be 833 km. The VIIRS scan will extend to 56 degrees on either side of nadir.

The VIIRS SRD places explicit requirements on spatial resolution for the Imagery EDR. Specifically, the Horizontal Spatial Resolution (HSR) of bands used to meet threshold Imagery EDR requirements must be no greater than 400 m at nadir and 800 m at the edge of the scan. This led to the development of a unique scanning approach which optimizes both spatial resolution and Signal to Noise Ratio (SNR) across the scan. The concept is summarized in Figure 2 for the imagery bands; the nested lower resolution radiometric bands follow the same paradigm at exactly twice the size. The VIIRS detectors are rectangular, with the smaller dimension projecting along the scan. At nadir, three detector footprints are aggregated to form a single VIIRS "pixel." Moving along the scan away from nadir, the detector footprints become larger both along track and along scan, due to geometric effects and the curvature of the Earth. The effects are much larger along scan. At around 32 degrees in scan angle, the aggregation scheme is changed from 3x1 to 2x1. A similar switch from 2x1 to 1x1 aggregation occurs at 48 degrees. The VIIRS scan consequently exhibits a pixel growth factor of only 2 both along track and along scan, compared with a growth factor of 6 along scan which would be realized without the use of the aggregation scheme. Figure 3 illustrates the benefits of the aggregation scheme for spatial resolution.

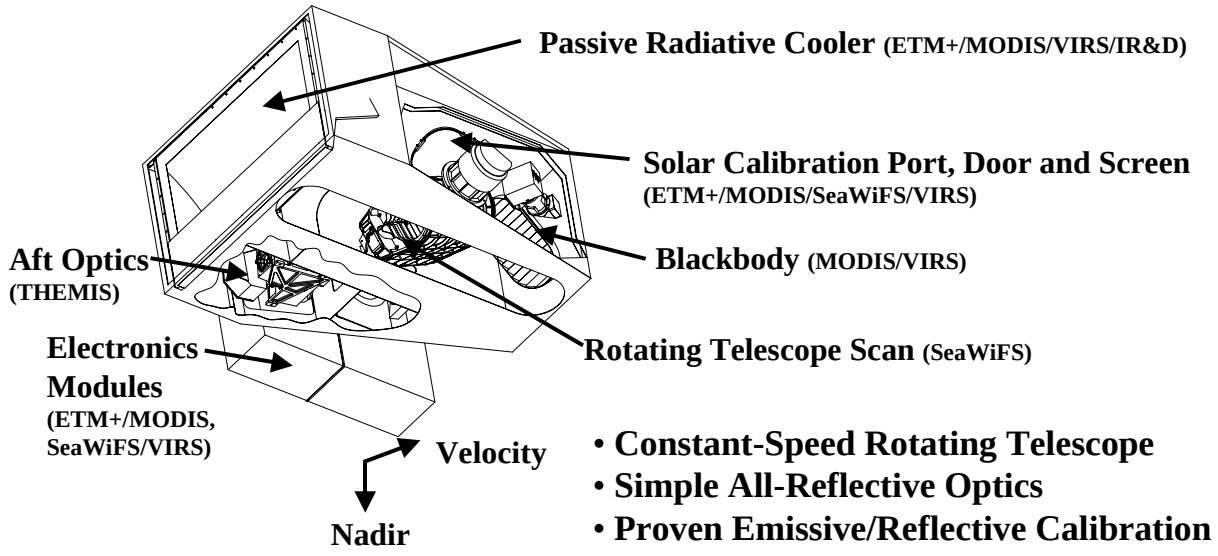

Figure 1. Summary of VIIRS design concepts and heritage.

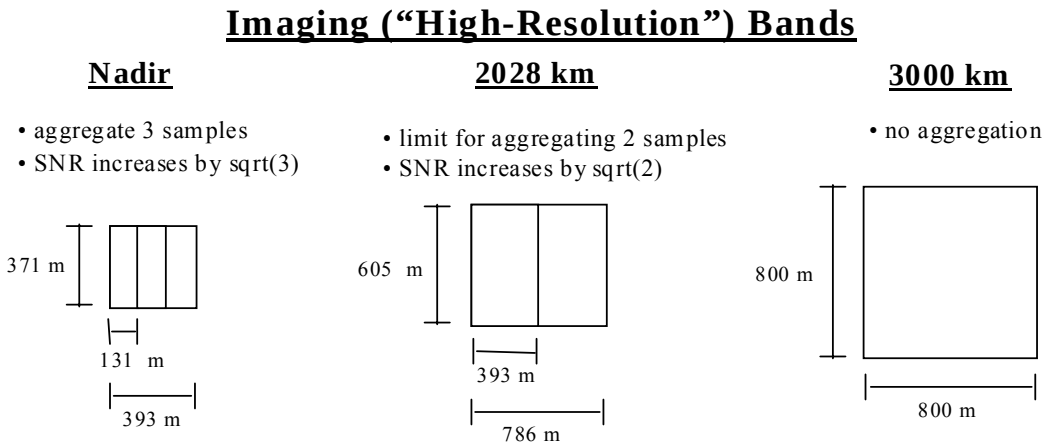

Figure 2. VIIRS detector footprint aggregation scheme for building "pixels." Dimensions are approximate.

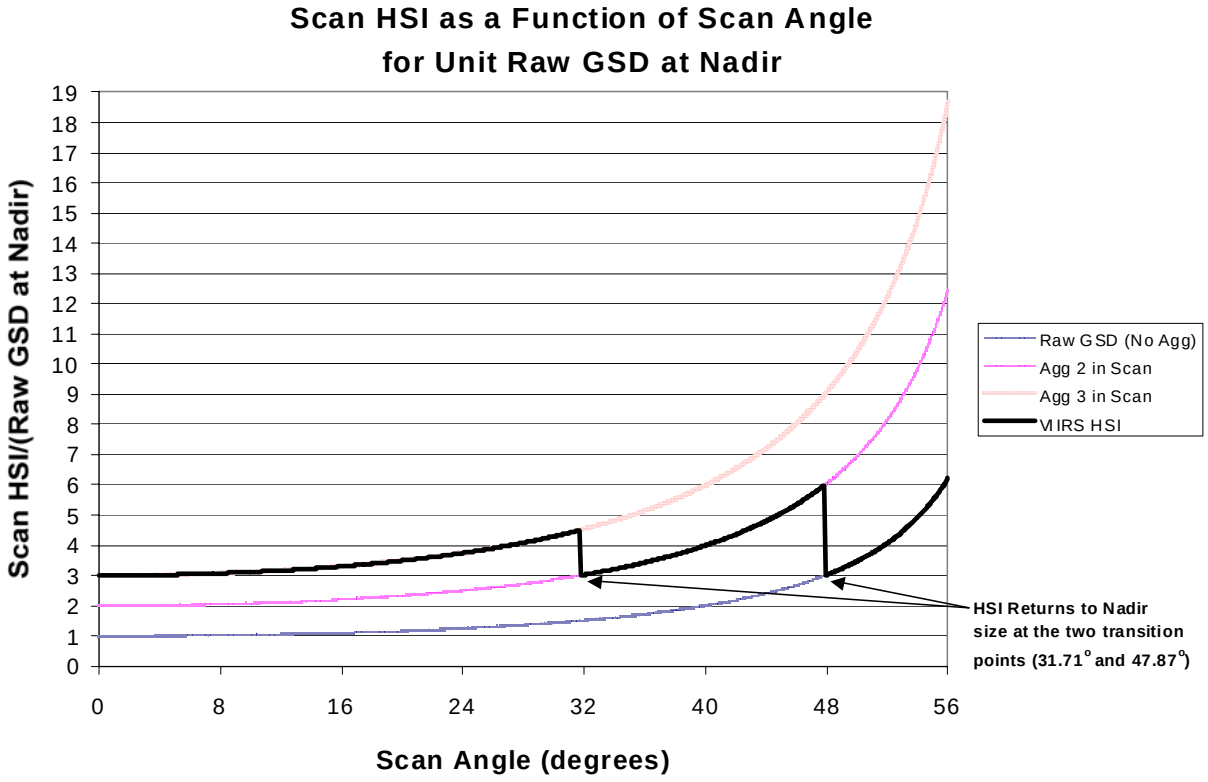

Figure 3. Benefits of VIIRS aggregation scheme in reducing pixel growth at edge of scan.

Table 1 summarizes the VIIRS bands. The positioning of the VIIRS spectral bands is shown in Figures 5 through 7.

Table 1. Bands included in the three primary VIIRS SDRs..

Band New	(Old)	Center (μm)	SDR_RAD	SDR_REF	SDR_BT	Notes
M1	(Chlor2)	0.412	X	X		Dual Gain
M2	(2)	0.445	X	X		Dual Gain
M3	(Chlor8)	0.488	X	X		Dual Gain
M4	(4)	0.555	X	X		Dual Gain
I1	(5i)	0.645	X	X		Imagery Resolution
M5	(Oc2)	0.672	X	X		Dual Gain
M6	(Oc3)	0.751	X	X		
I2	(6i)	0.865	X	X		Imagery Resolution
M7	(6r)	0.865	X	X	X	Emissive for Fires
M8	(Cloud1)	1.240	X	X	X	Emissive for Fires
M9	(7)	1.378	X	X		
I3	(8i)	1.610	X	X		Imagery Resolution
M10	(8r)	1.610	X	X	X	Emissive for Fires
M11	(9)	2.250	X	X		
M12	(10r)	3.700	X		X	
I4	(10i)	3.740	X		X	Imagery Resolution
M13	(Sst2)	4.050	X		X	Dual Gain
M14	(Sst4)	8.550	X		X	
M15	(11)	10.783	X		X	
I5	(12i)	11.450	X		X	Imagery Resolution
M16	(12r)	12.013	X		X	Dual Output
DNB		0.700	X	X		Day/Night Band

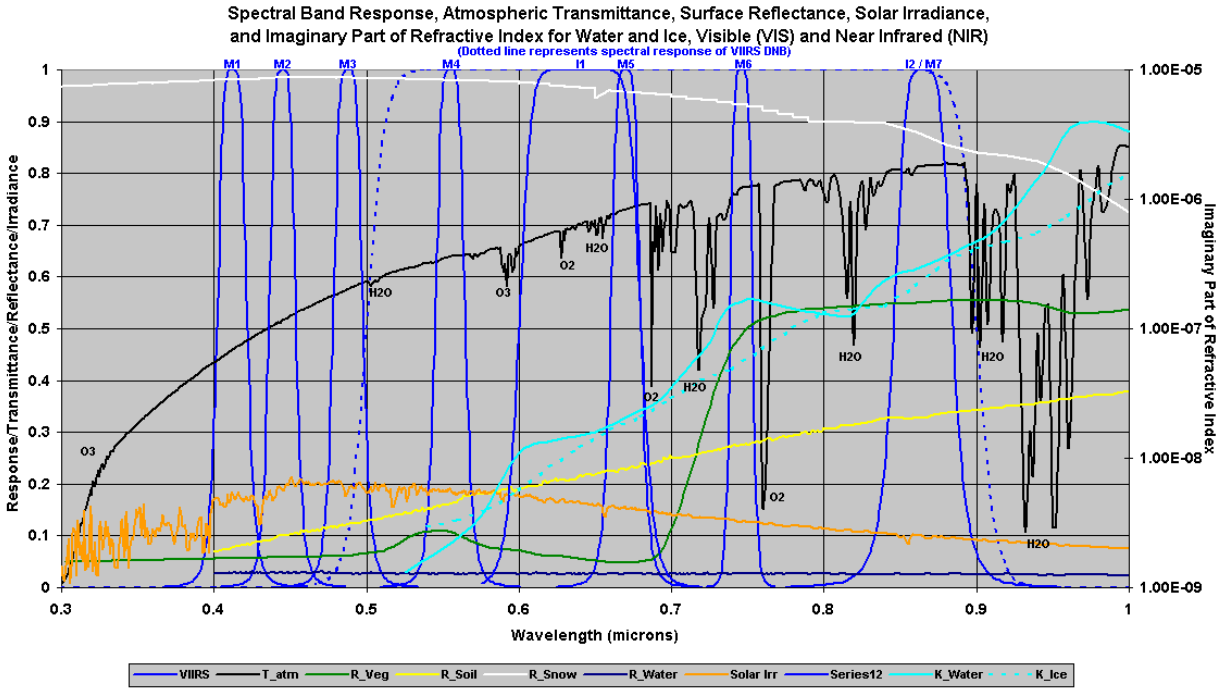

Figure 4. VIIRS spectral bands, visible and near infrared.

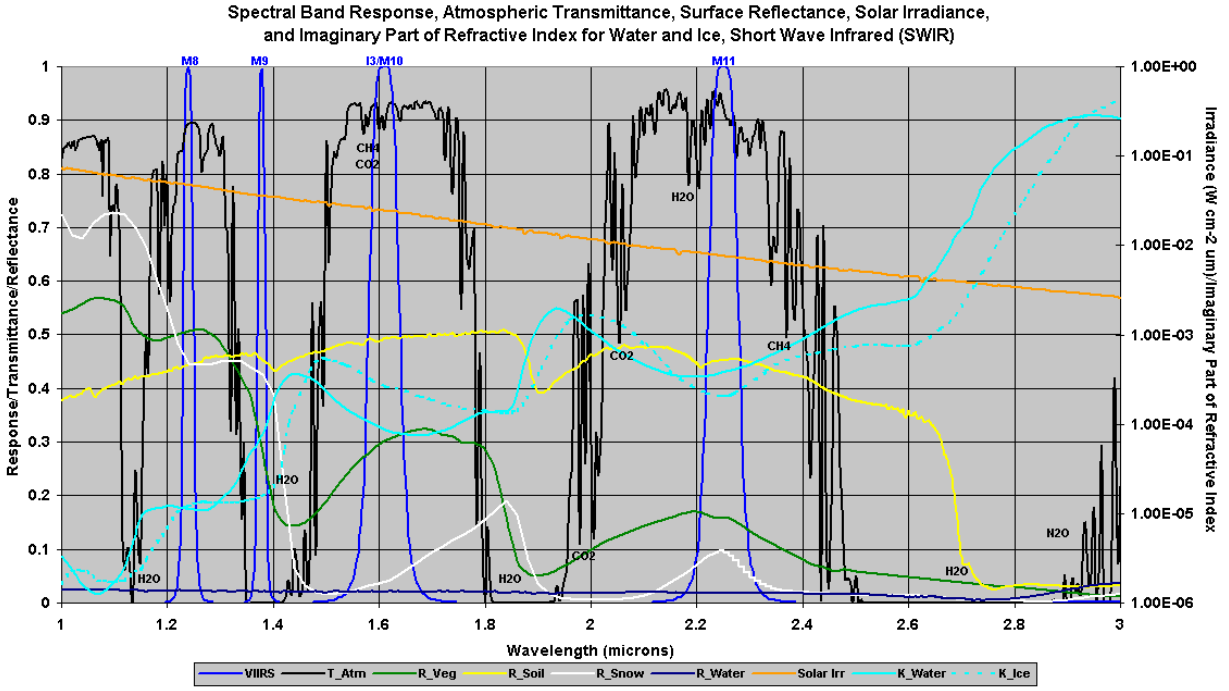

Figure 5. VIIRS spectral bands, short wave infrared.

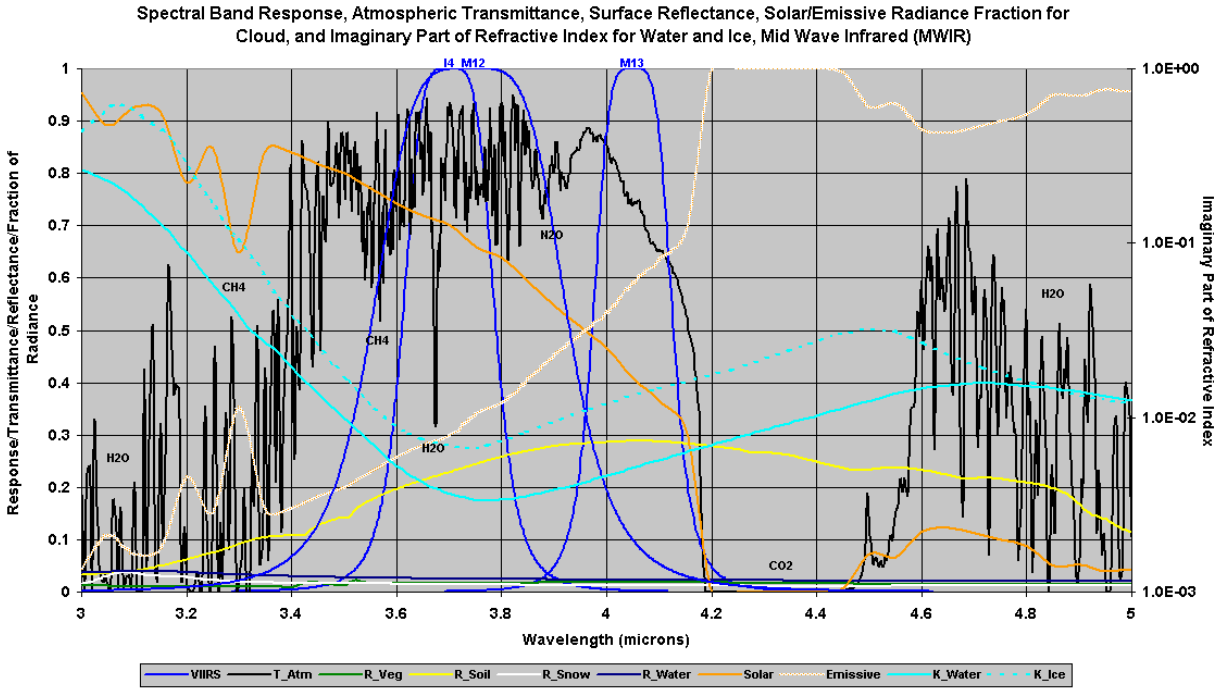

Figure 6. VIIRS spectral bands, medium wave infrared.

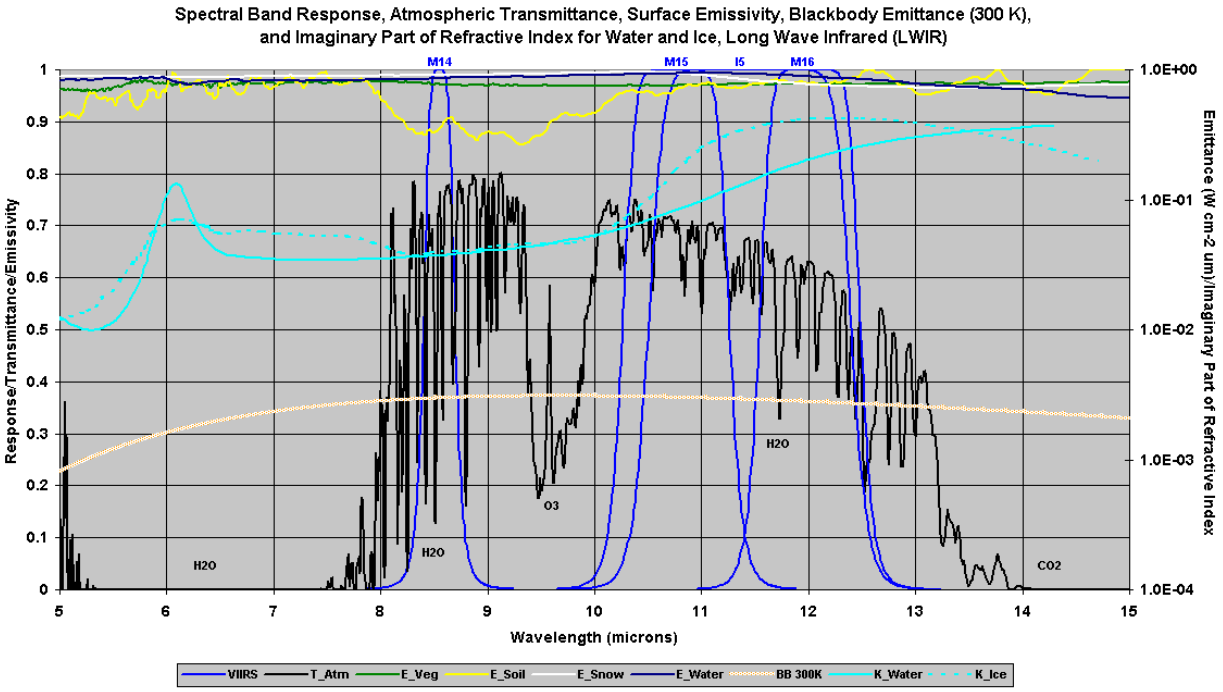

Figure 7. VIIRS spectral bands, long wave infrared.

2.3 RETRIEVAL STRATEGY

The PW EDR is essentially a non-linear function of earth and atmospheric parameters such as earth surface temperature, surface characteristics (emissivity and reflectivity), and temperature and water vapor profile conditions. VIIRS baseline infrared measurements are designed to be sensitive to all these elements that govern the PW EDR. For example, VIIRS shortwave infrared radiances are sensitive to surface parameters and less sensitive to water vapor absorption. Longwave VIIRS channels are, in contrast, sensitive to temperature and water vapor conditions. These two distinct measurement characteristics can provide a unique opportunity for VIIRS to retrieve PW with good performance and work toward higher performance using an enhanced VIIRS configuration. Raytheon's PW retrieval strategies uniquely take advantage of all available infrared radiances to obtain the PW EDR in a non-linear statistical "overlap regional" regression approach.

Since Raytheon's infrared retrieval uses the same algorithm and same input VIIRS data for both day and night, the retrieval system is relatively simple and no significant day/night biases will occur. The solar reflectance from the cloud and ground surfaces is explicitly accounted for during the retrieval process via a solar zenith angle term. The daytime PW EDR might have slightly better performance due to the fact that the solar reflectance provides additional information to complement the infrared thermal signal. It is expected that if the algorithm is capable of modeling the solar component signal accurately, the daytime PW retrieval will outperform its nighttime counterpart. Sensitivity studies of day and night PW retrievals will be presented in section 3.4.1.

The VIIRS PW EDR will use spectral bands at 3.7 μm, 4.05 μm, 8.55 μm, 10.76 μm, and 12.01 μm (M12, M13, M14, M15, M16) for all retrievals.

2.3.1 Clear Conditions

Clear PW retrievals are performed when the VIIRS Cloud Mask identifies a pixel as clear or probably clear. In this case, the retrievals are considered to cover the total column of PW integrated from the top of the atmosphere to the surface along the line of sight, using ancillary surface pressure data. The PW EDR is classified by temperature and humidity to improve performance. Sensitivity studies of clear retrievals are presented in section 3.4.1.

2.3.2 Cloudy Conditions

Cloudy PW retrievals are performed when the VIIRS Cloud Mask EDR identifies a pixel as cloudy or probably cloudy. Cloudy PW retrievals are considered to represent the PW from the top of the atmosphere to the top of the clouds along the line of sight. Sensitivity studies of cloudy retrievals will be presented in section 3.4.1.7.

3.0 ALGORITHM DESCRIPTION

3.1 PROCESSING OUTLINE

Figure 8 shows the top-level software architecture for the PW EDR. (The full description of the architecture is described in the VIIRS This Surface Temperature Module Level Software Architecture document *Y2473*). The PW EDR process starts with

- Read in pixel level cloud mask to determine clear, water cloud and non-water cloud PW processing path.
- Perform clear, water cloud or non-water cloud path PW retrieval with proper inputs.
    - Within each path, classification is performed to obtain the optimal class coefficient set to determine classified PW retrieval.
    - Near-real-time and static measurement inputs and ancillary data are assembled for retrieval.

A fast VIIRS infrared forward model is required for offline processing to generate regression coefficients. In addition, historical radiosonde profiles, which include measurements of temperature and water vapor, as well as surface skin temperature information, are required. Skin temperature can be estimated with the surface air temperature, but larger errors will result. The purpose of this processing is to generate non-linear regression coefficients to account for the statistical relationship between simulated VIIRS infrared radiances, PW, and surface emissivity. All the scenario parameters, such as sun/sensor geometry, surface pressure level, clear or cloud, and day/night information are essential for the analysis. Cloud mask input is required to select the clear or cloudy regression retrieval. All VIIRS baseline infrared channels from shortwave 3.7 μm to 12 μm are used along with the measurement noise estimates, forward model error, surface emissivity, aerosol absorption modeling and sub-cirrus cloud contamination.

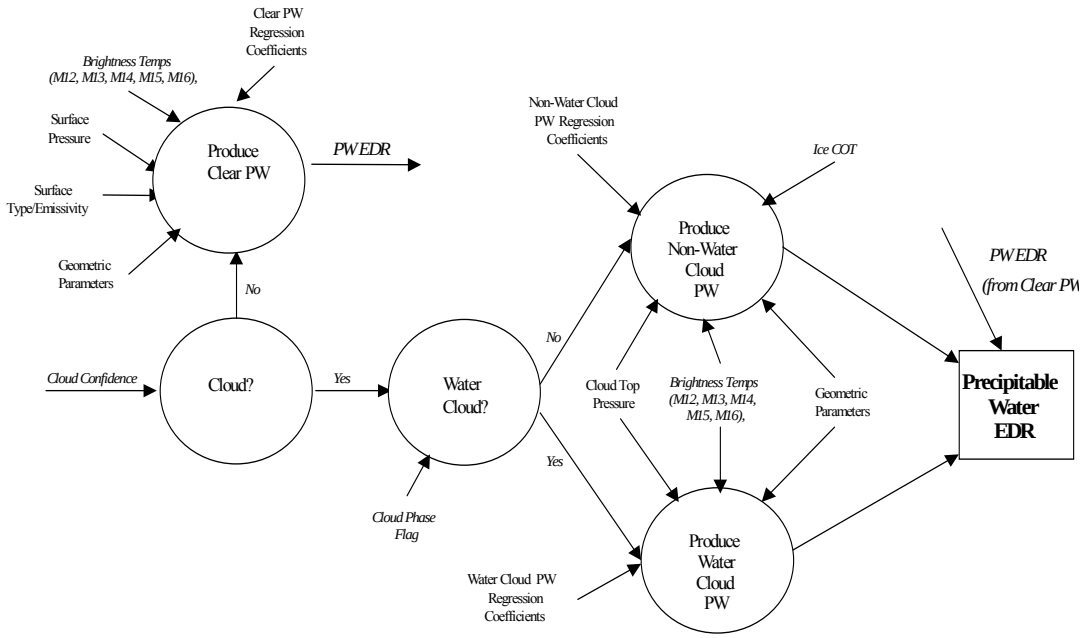

Figure 8. PW EDR software architecture.

3.2 ALGORITHM INPUT

3.2.1 VIIRS Data

The Top Of Atmosphere (TOA) calibrated brightness temperatures Sensor Data Record (SDR) is required for production of the VIIRS PW EDR. This SDR includes the necessary solar and viewing zenith angle information, along with geo-location parameters. The VIIRS cloud mask is required to define a clear or cloudy PW EDR retrieval. Pre-determined VIIRS surface emissivity information is also required to improve PW retrieval for various surface conditions. This is derived using the most recent output of the VIIRS Surface Type EDR.

3.2.2 Non-VIIRS Data

Near-real-time (at most a few hours old) surface pressure is the essential non-VIIRS data input to the retrieval of PW.

3.3 THEORETICAL DESCRIPTION OF RETRIEVALS

This section outlines the basic principles for obtaining PW based on the non-linear relationship between PW and VIIRS radiances, and it describes how the inverse problem can be physically and statistically formulated to accurately and efficiently deal with VIIRS PW processing at pixel resolution.

3.3.1 Physics of the Problem

Top of atmosphere VIIRS radiances represent very complicated physical processes of radiative transfer, which are involved with multiple atmospheric effects. These include temperature and

water vapor within the whole column path of the VIIRS Instantaneous Field of View (IFOV), underlying clouds, surface boundaries, thermal reflections, cloud/aerosol scattering, and gaseous absorption. The non-unique and non-linear aspects of the PW retrieval problem can be solved by a non-linear statistical regression approach.

3.3.1.1 Spectral Characteristics of PW

The dependence of the differences between brightness temperatures in different VIIRS channels on the amount of PW is shown in Figure 9 for both night and day. At night, brightness temperature differences between two VIIRS baseline shortwave channels display a nonlinear relationship with respect to the PW amount. A linear increase in PW does not correspondent to a linear increase in the two-channel difference. As a matter of fact, it is interesting to note the opposite sign in the relationship between low and high amounts of PW. Differences between the 8.55 and 11 μm channels also exhibit a nonlinear relationship; however, unlike the shortwave case, the differences increase with increasing PW amount. Longwave channel differences are much more linear with respect to the PW amount. The differences between shortwave and longwave channels produce much more scattered distributions due to the greater surface emissivity variations between these two spectral regimes. During the day, due to the solar reflectance, the differences in the two shortwave channels are dramatically different than for the nighttime case, with a wider spread and higher nonlinearity with the amount of PW. For other two-channel differences, no significant differences in behavior between day and night are observed. As expected, differences between shortwave and longwave bands still exhibit broad scatter features.

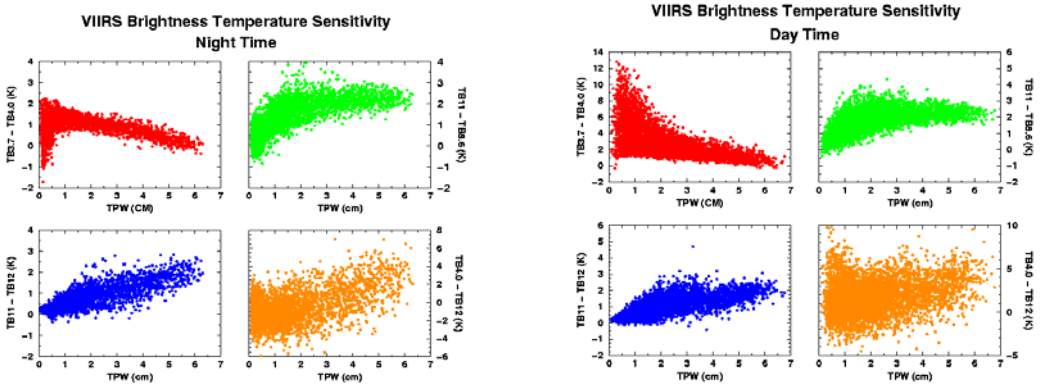

Figure 9. Scatter plots of VIIRS two-channel brightness temperature differences against PW amount.

That PW information exists in the VIIRS IR measurements is clearly demonstrated by the correlation plots between channel brightness temperatures and PW, shown in Figure 10. In general, water vapor channels sensitive to certain layers of atmospheric water vapor exhibit much lower correlations with PW when compared to channels with carbon dioxide (temperature) absorption information. It is very important to note that PW information embedded in VIIRS IR measurements is strongly dependent not only on integrated column water vapor, but also on the temperature profile. For example, PW correlation values range from 0.921 to 0.938 for carbon

dioxide channels and from 0.388 to 0.861 for water vapor channels. It is clear from these correlation plots that VIIRS PW retrievals can be incrementally improved if temperature-sensitive channels are incorporated into the instrument and the PW retrieval algorithm uses both water vapor and temperature channels simultaneously.

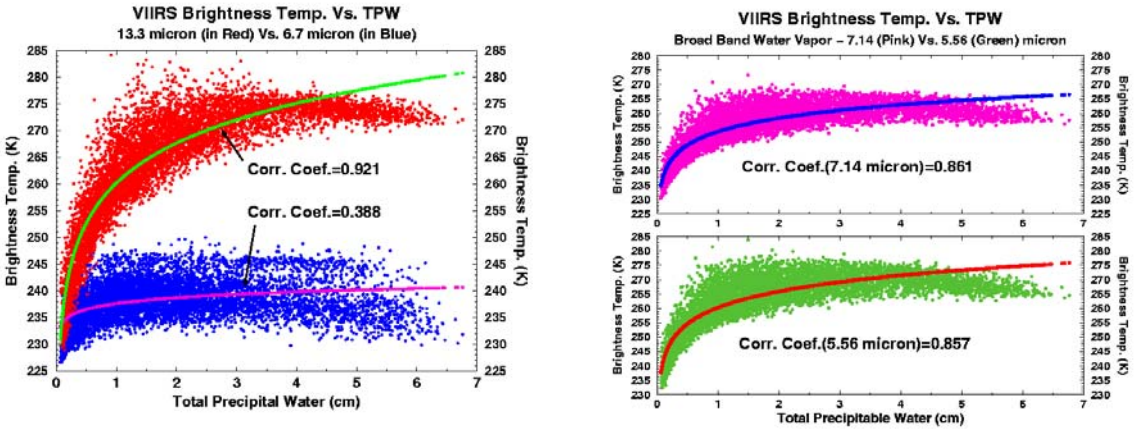

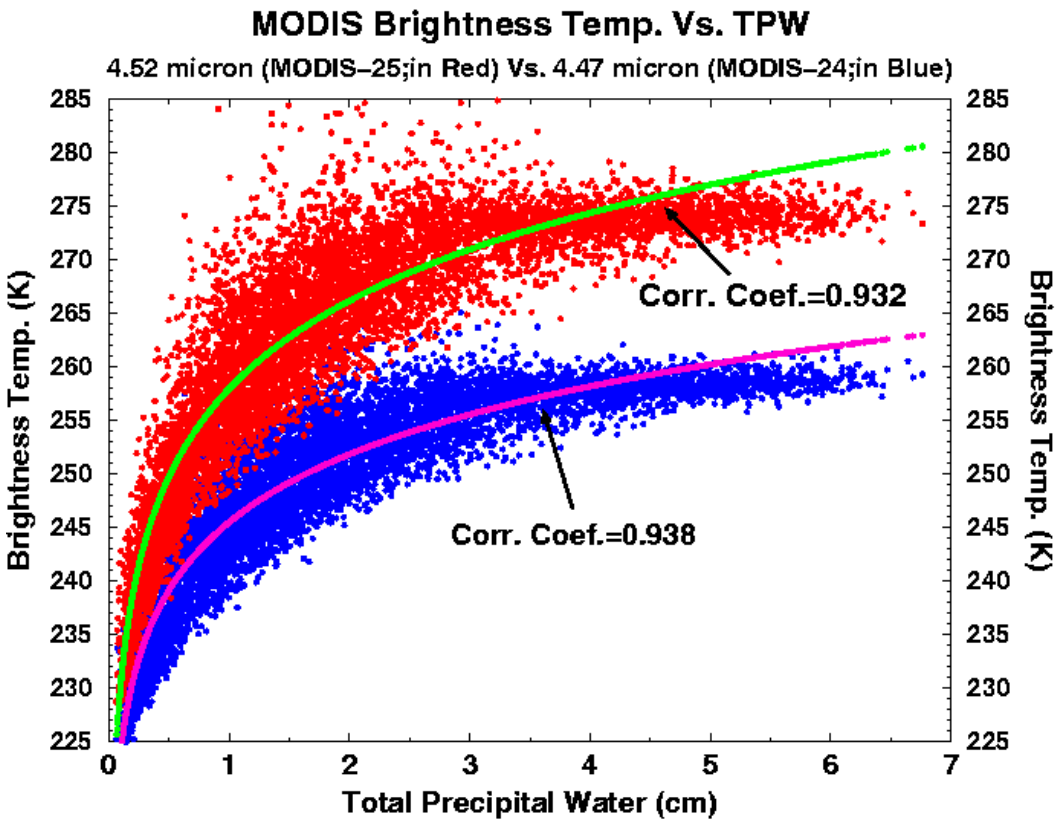

Figure 10. Correlation plots of IR temperature and water vapor channel brightness temperatures with PW amount.

3.3.1.2 Historical Development of PW Products

Determination of the total column PW is most directly accomplished by integrating the moisture profile through the atmospheric column. However, several simpler approaches are also viable. They are briefly described below.

The split window method can be used to specify total water vapor concentration from clear sky 11 μm and 12 μm brightness temperature measurements. The water vapor is evaluated by observing the area of interest in both infrared window bands. In the atmospheric window regions, the absorption is weak so that

$$\tau_w = e^{-K_w u} \approx 1 - K_w u \tag{1}$$

where w denotes the window band, K is the absorption coefficient, and u is the total column water vapor path. What little absorption exists is due to water vapor; therefore, u is a measurement of PW vapor. The measured radiance in the window region can be written from (2) if a blackbody surface is assumed

$$R_w = B_{sw}(1 - K_w u_s) + K_w \int_0^{u_s} B_w du \quad . \tag{2}$$

Defining an atmospheric mean Planck radiance

$$\overline{B}_w = \int_0^{u_s} B_w du \Big/ \int_0^{u_s} du \quad , \tag{3}$$

then

$$R_w = B_{sw}(1 - K_w u_s) + K_w u_s \overline{B}_w \quad . \tag{4}$$

Since B_{sw} is close to both R_w and B_w, a first order Taylor expansion about the surface skin temperature T_s allows us to linearize the RTE with respect to temperature, giving

$$T_{bw} = T_s(1 - K_w u_s) + K_w u_s \overline{T}_w \quad , \tag{5}$$

where $\overline{T}_w$ is the mean atmospheric temperature corresponding to B_w. This implies that

$$u_s = [T_{bw} - T_s] \Big/ [K_w(\overline{T}_w - T_s)] \quad . \tag{6}$$

Obviously, the accuracy of the determination of the total water vapor concentration depends upon the contrast between the surface skin temperature and the effective temperature of the

atmosphere. In an isothermal situation, the total PW vapor concentration is indeterminate. For two window spectral bands (11 μm and 12 μm) the split window approximation allows us to have

$$T_s = [K_{w2}T_{bw1} - K_{w1}T_{bw2}] \Big/ [K_{w2} - K_{w1}] \quad , \tag{7}$$

and if we express T_w as proportional to T_s

$$\overline{T}_w = a_w T_s \tag{8}$$

then a solution for u_s follows:

$$u_s = \frac{T_{bw2} - T_{bw1}}{(a_{w1} - 1)(K_{w2}T_{bw1} - K_{w1}T_{bw2})} = \frac{T_{bw2} - T_{bw1}}{b_1 T_{bw1} - b_2 T_{bw2}} \quad . \tag{9}$$

The coefficients b_1 and b_2 can be evaluated in a linear regression analysis from prescribed temperature and water vapor profile conditions coincident with in-situ observation of u_s. The weakness of this method is due to the time and spatial variability of a_w and the insensitivity of a stable lower atmospheric state $T_{bw1} - T_{bw2}$ to the total PW vapor concentration.

Another approach lies in the Split Window Variance Ratio, which starts from atmospheric windows with minimal moisture absorption

$$R_w = B_{sw}(1 - K_w u_s) + K_w u_s \overline{B}_w \quad .$$

Consider neighboring fields of view and assume that the air temperature is invariant. Then the gradients can be written

$$DR_w = DB_{sw}(1 - K_w u_s) \quad , \tag{10}$$

where D indicates the differences due to different surface skin temperature in the two FOVs. Convert to brightness temperatures with a Taylor expansion with respect to one of the surface skin temperatures, so that

$$[R_w(FOV1) - R_w(FOV2)] = [B_{sw}(FOV1) - B_{sw}(FOV2)](1 - K_w u_s) \quad , \tag{11}$$

$$[T_w(FOV1) - T_w(FOV2)] = [T_s(FOV1) - T_s(FOV2)](1 - K_w u_s) \, . \tag{12}$$

Using the split windows can provide an estimate for u_s in the following way. Write the ratio

$$\begin{aligned}\frac{1-K_{w1}u_s}{1-K_{w2}u_s} &= \frac{dR_{w1}dB_{sw2}}{dR_{w2}dB_{sw1}} \\ &= \frac{[R_{w1}(FOV1)-R_{w1}(FOV2)][B_{sw2}(FOV1)-B_{sw2}(FOV2)]}{[R_{w2}(FOV1)-R_{w2}(FOV2)][B_{sw1}(FOV1)-B_{sw1}(FOV2)]} \\ &= \frac{[T_{w1}(FOV1)-T_{w1}(FOV2)][T_s(FOV1)-T_s(FOV2)]}{[T_{w2}(FOV1)-T_{w2}(FOV2)][T_s(FOV1)-T_s(FOV2)]} \\ &= \frac{[T_{w1}(FOV1)-T_{w1}(FOV2)]}{[T_{w2}(FOV1)-T_{w2}(FOV2)]}\end{aligned} \tag{13}$$

The surface skin temperature cancels out, so

$$\frac{1-K_{w1}u_s}{1-K_{w2}u_s} = \frac{DT_{w1}}{DT_{w2}}, \tag{14}$$

or

$$u_s = (1-D_{12})/(K_{w1}-K_{w2}D_{12}), \tag{15}$$

where D_{12} represents the ratio of the deviations of the split window brightness temperatures. The deviation is often determined from the square root of the variance.

The assumption in this technique is that the difference in brightness temperatures from one FOV to the next is due only to the different surface skin temperatures. It is best applied to an instrument with relatively good spatial resolution, so that sufficient samples can be found in an area with small atmospheric variations and measurable surface variations in order to determine the variance of the brightness temperatures accurately. The technique was suggested by the work of Chesters et al. (1983) and Kleespies and McMillin (1984). Jedlovec (1987) successfully applied it to aircraft data with 50 m spatial resolution to depict mesoscale moisture variations preceding thunderstorm development.

MODIS split window algorithm

The split window method can be used to specify total PW from clear sky 11 μm and 12 μm brightness temperatures. In the atmospheric window channels, the absorption is weak so that

$$\tau_i = \exp(-k_i w \sec\theta) \approx 1 - k_i w \sec\theta \tag{16}$$

where i denotes the channel index and w is the total PW; hence

$$d\tau_i = -k_i \sec\theta \, dw \tag{17}$$

In a window channel, there is little absorption due to water vapor; therefore, w is a measure of column water vapor. The measured radiance in the thermal window region can be written from the RTE

$$R_i = \varepsilon_i B_i(T_s)\tau_i + \int_0^{\tau} B_i(T(p))d\tau \qquad (18)$$
$$= \varepsilon_i B_i(T_s)(1 - k_i w \sec\theta) + k_i \sec\theta \int_0^{W} B_i(T(p))dw$$

where W represents the total column water vapor or PW. Defining an atmospheric mean Planck radiance

$$B_i(T_a) = \int_0^{W} B_i(T(p))dw \Big/ \int_0^{W} dw \qquad (19)$$
$$R_i = \varepsilon_i B_i(T_s)(1 - k_i W \sec\theta) + k_i \sec\theta W B_i(T_a)$$

the Planck function can be expanded in a Taylor series about the brightness temperature T_i in the form of

$$R_i = B_i(T_i) = \frac{DB}{DT}|_{T_i} \frac{B_i(T_i)}{\frac{DB}{DT}|_{T_i}} = \frac{DB}{DT}|_{T_i} L(T_i) \qquad (20)$$

$$B_i(T_s) = B_i(T_i) + \frac{DB}{DT}|_{T_i} (T_s - T_i) = \frac{DB}{DT}|_{T_i} (T_s - T_i + L(T_i))$$

$$B_i(T_a) = B_i(T_i) + \frac{DB}{DT}|_{T_i} (T_a - T_i) = \frac{DB}{DT}|_{T_i} (T_a - T_i + L(T_i))$$

It can allow us to linearize the RTE with respect to temperature, so

$$L(T_i) = \varepsilon_i (1 - k_i w \sec\theta)(T_s - T_i + L(T_i)) + k_i w \sec\theta (T_a - T_i + L(T_i)) \qquad (21)$$

Several approximations have been proposed for $L(T_i)$. Among one of them is

$$L(T_i) = T_i / n_i \qquad (22)$$

With this expression, total PW can be expressed as

$$W = \frac{(C_{i1} T_i - \varepsilon_i T_s)\cos\theta}{k_i (T_a - \varepsilon_i T_s - C_{i2} T_i)} \qquad (23)$$

where

$$C_{i1} = \frac{1 + (n_i - 1)\varepsilon_i}{n_i}, \; C_{i2} = \frac{(n_i - 1)(1 - \varepsilon_i)}{n_i}$$

$\varepsilon_i \approx 1.0$

For ocean, the emissivity at 11 μm and 12 μm is essentially unity.

$$W = \frac{T_i - T_s}{k_i \sec\theta (T_a - T_s)} \tag{24}$$

Surface temperature (T_s) over ocean and for a specific surface type can be derived as (see VIIRS SST or LST ATBD)

$$Ts = T_1 - (T_2 - T_1) k_1 / (k_2 - k_1) = \frac{k_2 T_1 - k_1 T_2}{(k_2 - k_1)} \tag{25}$$

And if we assume T_a is proportional to T_s

$$Ta = a_w Ts \tag{26}$$

Then a solution for W can be expressed as:

$$W = \frac{(T_2 - T_1)\cos\theta}{(a_w - 1)(k_2 T_1 - k_1 T_2)} = \frac{(T_2 - T_1)\cos\theta}{b_1 T_1 - b_2 T_2} \tag{27}$$

This is the MODIS PW algorithm. As seen from our derivation, this algorithm can only be used over ocean. Otherwise, the assumption that T_a is proportional to T_s may lead to large errors.

3.3.2 Mathematical Description of the VIIRS Algorithm

As shown in section 3.3.1.2, the historical PW algorithm uses a split-window approach. Although many shortwave and longwave IR radiance channels are simultaneously available, only two longwave IR window channels are utilized. From figure 10 of 3.3.1.1 (spectral characteristics of PW), we demonstrate that many other IR channels exhibit excellent correlation with PW in a non-linear way. By taking advantage of VIIRS multiple IR radiance measurements, a non-linear regression approach can also be applied to VIIRS data for PW retrieval. This procedure is based on either a single FOV's measurements or averaged measurements within FOVs. All infrared window spectral bands can be use in this procedure. For example, the PW can be derived by

$$PW = a_0 + \sum_{i=1}^{NB} a_i Tb_i + \sum_{i=1}^{NB}\sum_{j=i}^{NB} c_{ij} Tb_i Tb_j + d_1 \sec\theta + d_2 p_s + d_3 \cos(\Phi) + d_4 Emis\,, \tag{28}$$

where Tb_i is the brightness temperature for the ith spectral band, p_s is the surface pressure, θ and Φ are the satellite local zenith angle and solar zenith angle, respectively. *Emis* is surface emissivity, to account for the effects of different surface types. In the case of water cloud, *Emis* is the water cloud emissivity and will be pre-set to unity. For ice cloud, *Emis* is derived from ice Cloud Optical Thickness (COT), an output of the cloud module. NB is the total number of VIIRS spectral bands used. a, c and d are the regression coefficients. Equation (28) illustrates how PW can be inferred from the VIIRS infrared window band measurements with the addition

of surface and angle information. The quadratic term is indicative of the nonlinear relationship in the regression between PW and VIIRS IR window spectral band radiances.

VIIRS measurement noise is explicitly accounted for by adding appropriately scaled random noise to the brightness temperatures in the regression equation. For PW EDR retrieval under cloudy conditions, eq. (28) can be generalized as well. The input cloud height and cloud emissivity will replace P_s and *Emis* to account for the cloud effects. Furthermore, eq. (28) can be applied to temperature- and humidity-dependent atmospheric conditions to obtain classified regression coefficient sets, which will improve PW retrieval performance. A demonstration of this improvement using the "overlap regional" approach is presented in section 3.4.1.6.

3.3.3 Archived Algorithm Output

PW retrieval outputs include geo-location, PW values, and quality flags indicating which class of retrieval is performed and whether the unclassified and classified PW difference is reasonably small. The output is retained within the VIIRS processing stream for use by other algorithms, such as Surface Reflectance.

3.3.4 Variance and Uncertainty Estimates

Table 2 lists the requirements specified for the PW EDR.

Table 2. VIIRS System Specification prescribed requirements for the PW EDR.

Requirement Number	Parameter	Requirement
SSV0482	EDR PREWTR HCS at nadir	0.75 km
SSV0483	EDR PREWTR HRI	HCS
SSV0484	EDR PREWTR Horizontal Coverage	Global
SSV0485	EDR PREWTR Measurement Range	0 to 100 mm
SSV0486	EDR PREWTR Measurement Uncertainty, PW ≥ 5 mm, clear, land	30%
SSV0487	EDR PREWTR Measurement Uncertainty, PW ≥ 5 mm, clear, ocean	20%
SSV0838	EDR PREWTR Measurement Uncertainty, PW ≥ 5 mm, cloudy	32%
SSV0839	EDR PREWTR Measurement Uncertainty, PW < 5 mm, clear	1.5 mm
SSV0840	EDR PREWTR Measurement Uncertainty, PW < 5 mm, cloudy	1.5 mm
SSV0489	Minimum Swath Width (All other EDR thresholds met)	3000 km

MODIS data will allow a new level of performance to be achieved in PW retrievals. However, this level is difficult to define without actual application of the MODIS algorithm to real data, and validation using long term co-located in-situ and retrieved PW.

3.4 ALGORITHM SENSITIVITY STUDIES

The VIIRS PW non-linear regression retrieval sensitivity was studied using the simulation procedure described below. The PW accuracy and precision were calculated from several components of uncertainty, including measurement error, forward model error, temperature and water vapor profile uncertainties, surface emissivity and reflectivity uncertainty, cloud height

uncertainty, sub-visible cirrus cloud contamination, and aerosol contamination. Improvement due to the inclusion of an additional, temperature-sensitive, carbon dioxide spectral band is also studied.

3.4.1 Description of Simulations

In order to derive the regression coefficients, VIIRS infrared window band radiances are calculated from two sets (February for winter and August for summer) of global radiosonde profiles. These profiles include atmospheric temperature, moisture and ozone. A fast atmospheric transmittance model, Pressure Layer Optical Depth (PLOD) (Hannon et al., 1996), is used for the radiative transfer calculations. PLOD uses 42 vertical pressure levels ranging from 0.1 to 1050 mb. The VIIRS instrument noise plus an assumed 0.2K forward model error is added onto the simulated VIIRS infrared band radiance. The PW regression coefficients and EDR are generated based on the following two configurations:

1) Global Regression Coefficients Generation and PW Retrieval

Two sets of historical global profiles (dependent samples of 8647 and 8342, respectively) are used to generate the regression coefficients. These coefficients are then applied to the simulated VIIRS spectral measurements for the months of February and August of 2001 (independent samples of 717 and 743, respectively) to obtain the PW retrievals. The precision expressed in terms of total column PW error in percent is defined as

$$Precision = 100\% \times \sqrt{\frac{1}{NS}\sum_{j=1}^{NS}\left(\frac{PW_j^{true} - PW_j^{rtv}}{PW_j^{true}}\right)^2}\ , \qquad (29)$$

where PW^{true} and PW^{rtv} are "true" PW and regression derived retrieval values respectively, and NS is the number of independent cases. The two dependent training global profile sets used in the global unclassified PW retrieval coefficient generation are as follows: set 1 consists of 8647 profiles from January, February, and March of 2000 plus January of 2001; set 2 consists of 8342 profiles from July, August and September of 2000 plus July of 2001. Sections 3.4.1.1 and 3.4.1.6 compare the global PW retrieval uncertainty with the results of classified PW retrieval, using the scheme described below.

A set of global PW regression retrieval coefficients should be updated each month using 4 months of global radiosonde profiles. The 4-month period consists of the preceding, current, and following month of the previous year and the preceding month of the current year. The selection of such 4-month samples is described in the next section.

2) Overlap Regional Classified Regression Coefficients

In this scheme, each of the two dependent and independent sets of global retrievals described above is classified into six (6) sub-classes based on the simulated VIIRS 11 μm band brightness temperature, as defined in Table 3. Note that the training intervals are wider than the retrieval intervals – hence the term "overlap regional" classification. The 10 K overlap between

neighboring classes is beneficial for retrieval of the PW EDR when an incorrect class coefficient set is selected because of excessive measurement noise of Tb(11).

Table 3. VIIRS simulated 11 μm brightness temperature intervals for overlap regional regression classification

Class	Nominal Range (K) for Classification	Actual Range (K) for Training
1	Tb <240	Tb<245
2	240≤Tb<255	235≤Tb<260
3	255≤Tb<270	250≤Tb<275
4	270≤Tb<285	265≤Tb<290
5	285≤Tb<300	280≤Tb<305
6	Tb≥300	Tb≥295
Note that Tb stands for the brightness temperature of VIIRS 11 μm band		

In summary, the joint use of portions of the dependent (or training) samples among the neighboring classes minimizes the PW EDR retrieval uncertainty for outlier pixels (those which possess much larger than normal measurement noise). Even if such an outlier pixel is assigned to the wrong class, the resulting PW retrieval will still be useful. This concept is one of the unique aspects of this newly proposed VIIRS multiple channel non-linear PW retrieval algorithm.

After successful classification, the set 1 and set 2 classified coefficients are then applied to the February and August 2001 simulated VIIRS measurements, respectively, for the baseline PW EDR retrieval analysis reported in this ATBD. These six sets of classified PW regression retrieval coefficients should be updated every month, in the same fashion as described above for the global unclassified regression coefficients.

3.4.1.1 Measurement noise sensitivity

VIIRS PW retrieval sensitivity towards measurement noise is demonstrated in Figure 11. A noise factor of 1 means PW is derived from the specification for VIIRS sensor noise. A noise factor of 0.2 essentially represents very high precision VIIRS measurements and noise factor of 2 implies the noise has been increased two times. PW retrieval precision, expressed in terms of percent error, is shown to be a nearly linear function of the noise factor, but the relationship is

not very strong. Unclassified (PW retrieved using the global coefficient set) and classified global PW retrievals were also investigated and found to have similar sensitivity to the measurement noise.

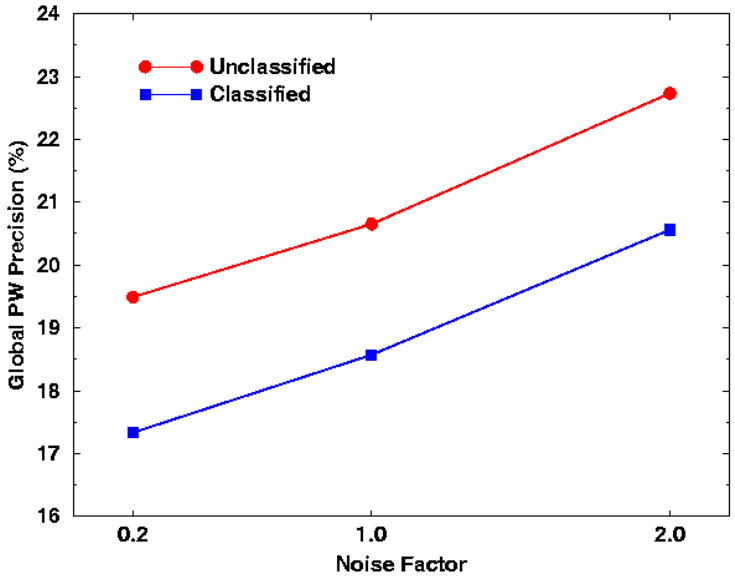

Figure 11. PW retrieval sensitivity to sensor noise (Noise factor of 1 is equal to the VIIRS spec. noise).

3.4.1.2 Carbon dioxide band sensitivity

As discussed in section 3.3.1.1, carbon dioxide channels are highly correlated with PW and would provide additional PW retrieval information on top of baseline VIIRS measurement capability. Figure 12 demonstrates global PW retrievals using the baseline VIIRS bands combined with other possible bands to enhance performance. A carbon dioxide band can indeed provide additional PW information, and a 4.52 μm band seems to provide the best retrieval precision when compared with baseline performance.

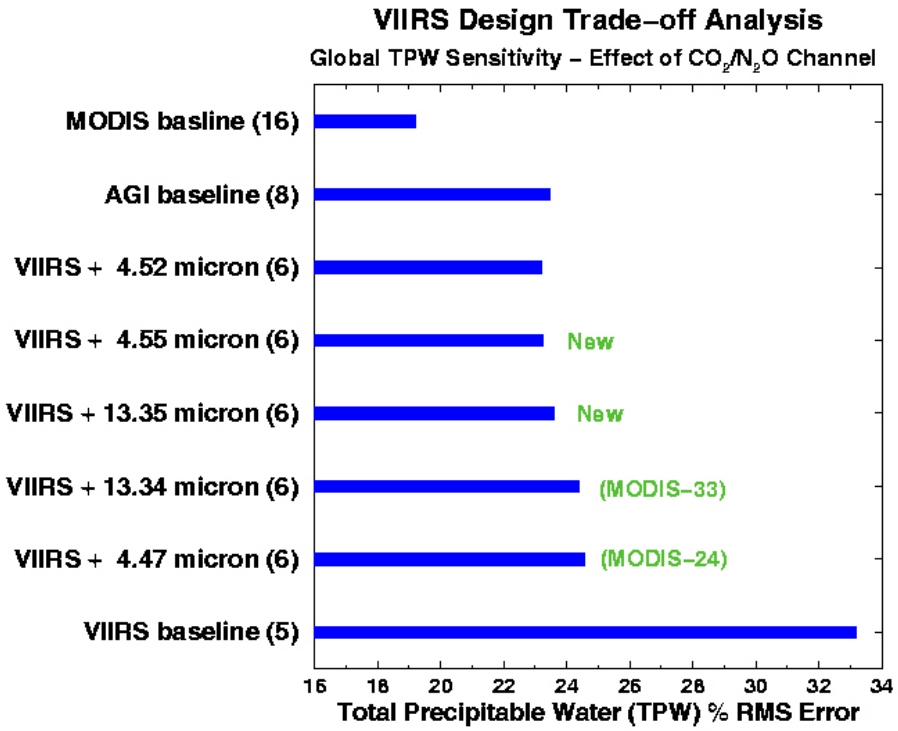

Figure 12. Trade study on optimal band combinations for precipitable water retrieval. "VIIRS" means the VIIRS baseline. Number within parentheses is the number of channels used in this PW retrieval trade-off analysis.

Figure 13 also demonstrates the enhancement of PW retrieval precision due to the addition of the carbon dioxide 4.5 μm band for four different region scenes in addition to the global scene shown in the previous figure. These four scenes were simulated from September 13-14, 1998 using CAMEX-3 NAST-I retrieved soundings. NAST-I PW was used as "truth" to assess the VIIRS PW precision for baseline and baseline plus 4.5 μm band instrument configurations. For the present, the VIIRS baseline will remain in its current configuration, without the addition of the 4.5 μm band. This decision emerged from a cost versus performance analysis conducted by the algorithm and sensor teams. Room for spare bands does exist, however, and the issue may be revisited in the future. It should be noted that the present VIIRS baseline performs quite well with regard to PW retrievals.

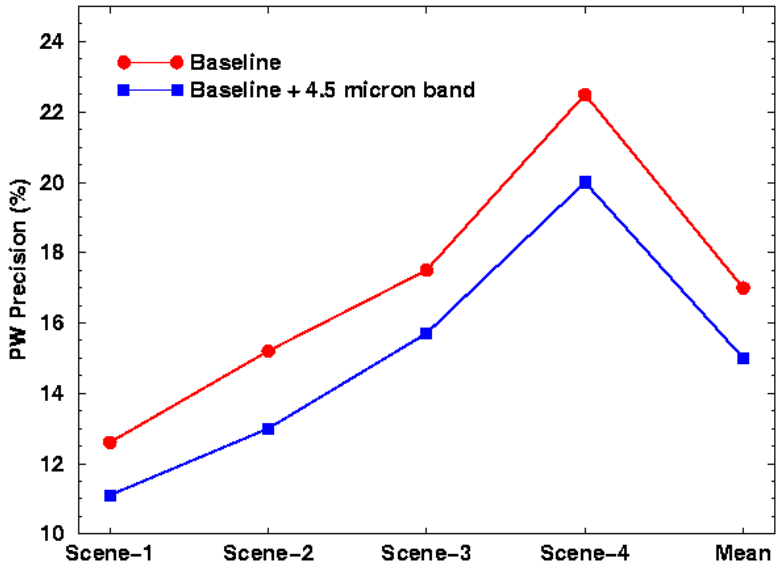

Figure 13. Utility of adding a 4.5 µm band to the VIIRS baseline for PW retrievals.

3.4.1.3 Land and Ocean surface sensitivity

Figure 14 shows how surface emissivity variations can affect brightness temperature in the five baseline bands used by the PW algorithm. Over oceans, a 0.5% emissivity variation is typical, while over land a few percent in emissivity variation is possible. These results indicate why an emissivity term is necessary in the regression equation.

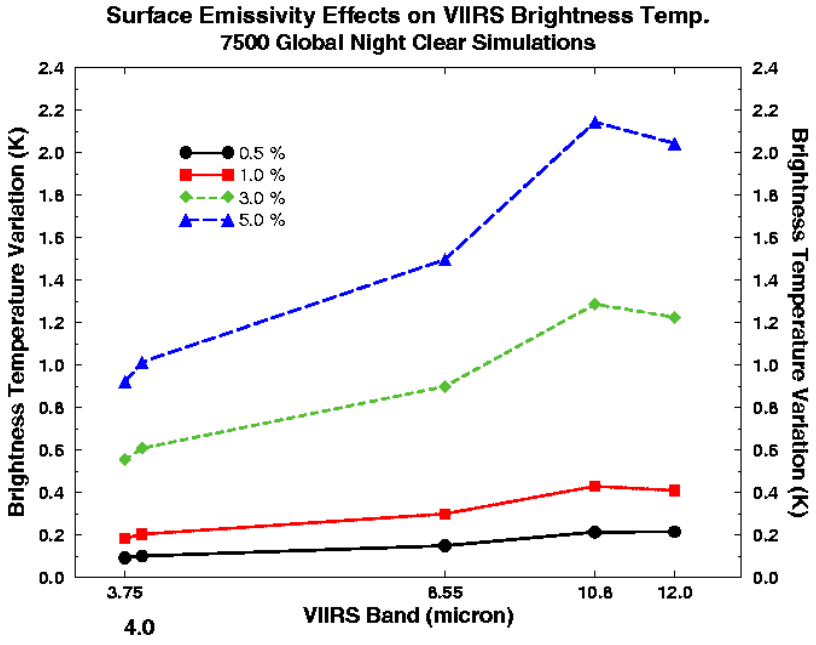

Figure 14. VIIRS brightness temperature variations due to changes in surface emissivity.

The resulting surface emissivity uncertainty can degrade the PW retrieval precision if its effects are not accounted for. Figure 15 shows the PW retrieval uncertainty over land and ocean surfaces, using different combinations of bands. Over land surfaces, a 3% surface emissivity uncertainty is assumed. Over oceans, 0.5% emissivity error is assumed. Obviously, better knowledge of emissivity or smaller surface emissivity variations will result in a more accurate PW retrieval.

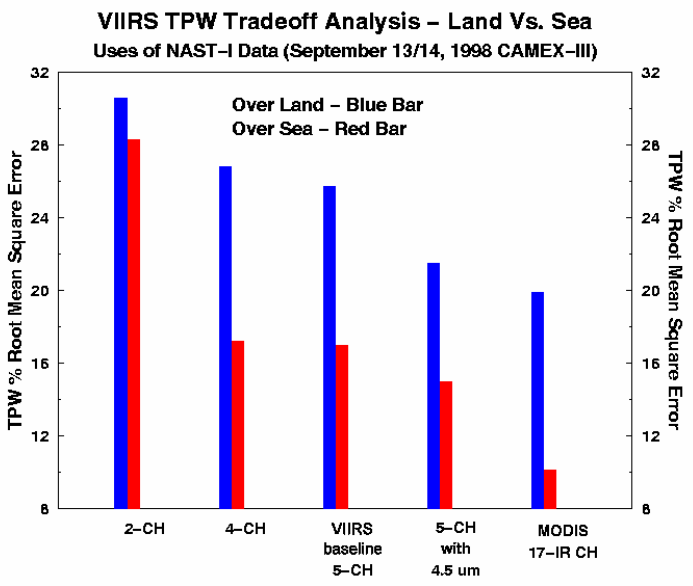

Figure 15. PW EDR algorithm performance for land and ocean surfaces.

Figures 16 and 17 further demonstrate the VIIRS baseline 5-band classified PW EDR retrieval uncertainty due to different surface emissivity variation and uncertainty of land and ocean surfaces. During winter daytime (January of 2001), Northern Hemisphere PW has uncertainty of 30.9% over ocean and 33.7% over land. During winter nighttime, Northern Hemisphere PW has uncertainty of 32.3% over ocean and 34.7 % over land. Similarly, during summer daytime (August of 2001), Northern Hemisphere PW has uncertainty of 24.1% over ocean and 25.2% over land. During summer nighttime Northern Hemisphere PW has uncertainty of 25.3% over ocean and 27.1% over land surface. In summary, PW retrieval over the ocean outperforms PW retrieval over the land because surface emissivity is well characterized for the ocean surface.

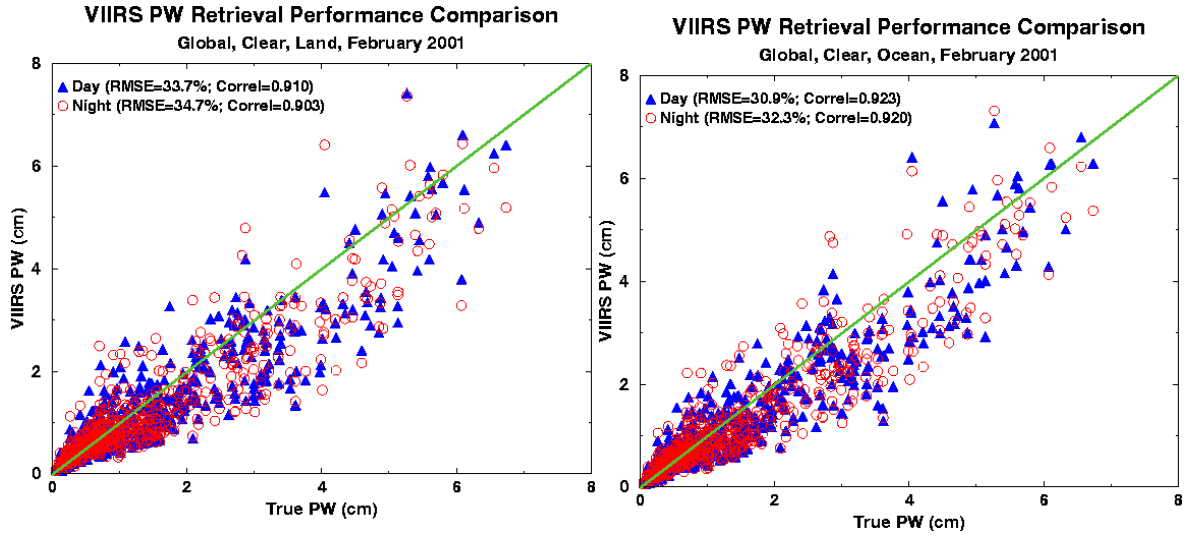

Figure 16. Northern Hemisphere winter (February of 2001) PW EDR retrieval sensitivity to land (left panel) and ocean (right panel) surfaces.

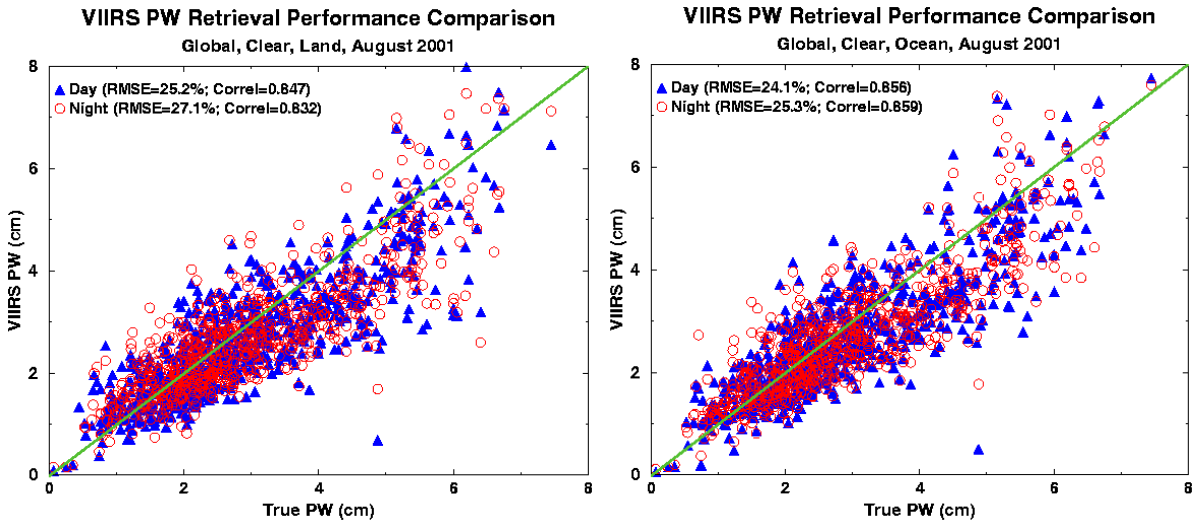

Figure 17. Northern Hemisphere summer (August of 2001) PW EDR retrieval sensitivity to land (left panel) and ocean (right panel) surfaces.

From Table 4, it is evident that PW EDR performance is better over ocean because of its much greater uniformity in surface characteristics compared to land.

Table 4. PW EDR performance over land vs. ocean (RMSE).

Case		Ocean	Land	Difference (Land-Ocean)
February	Day	30.9%	33.7%	2.8%
	Night	32.3%	34.7%	2.4%
August	Day	24.1%	25.2%	1.1%
	Night	25.3%	27.1%	1.8%
Note that in winter and over daytime PW has largest EDR performance contrast for two types of surface				

3.4.1.4 Aerosol contamination sensitivity

Two types of aerosol, namely maritime and continental, were modeled in the PW retrieval sensitivity studies. Figure 18 demonstrates the brightness temperature depression due to aerosol absorption.

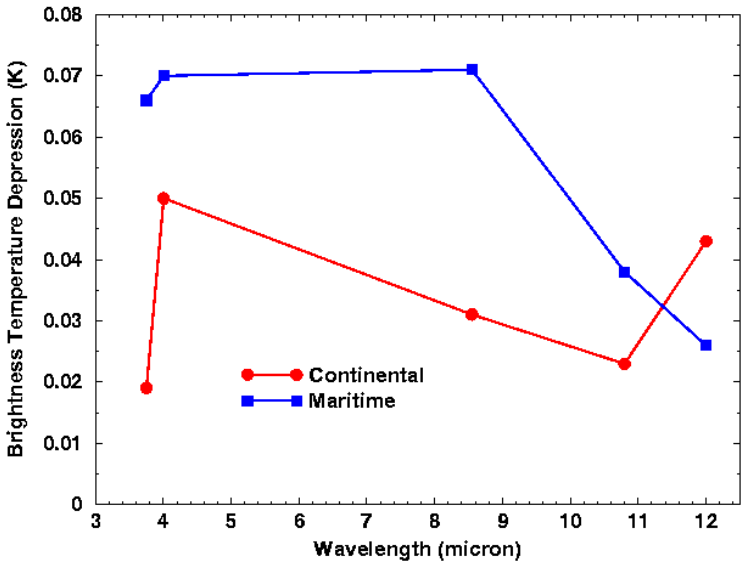

Figure 18. Brightness temperature depression due to absorption by continental or maritime aerosol.

Figure 19 shows that both types of aerosol can degrade the PW retrieval, but only very slightly for typical Aerosol Optical Thickness (AOT). Aerosol effects on unclassified and classified PW retrievals are almost the same. Aerosol detection and correction prior to PW retrieval can improve PW performance.

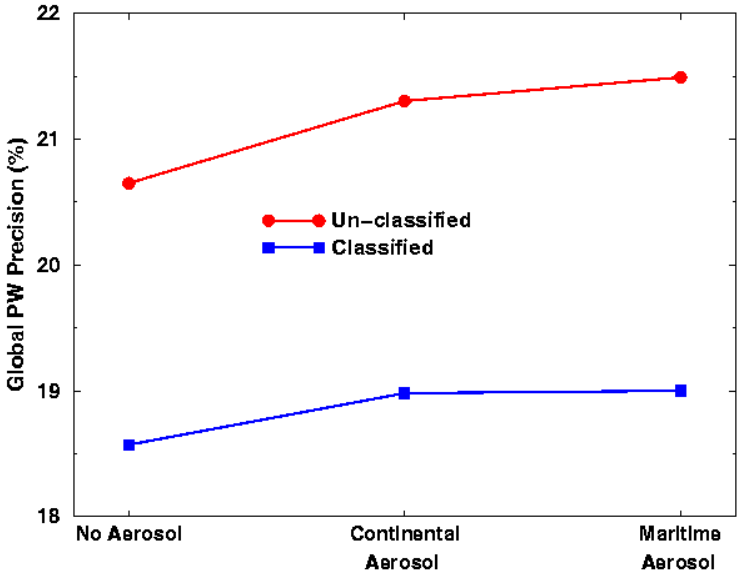

Figure 19. Aerosol effects on PW retrieval precision. Red line shows errors when air mass is unclassified; blue line shows results when classification is done.

3.4.1.5 Sub-visible cirrus cloud contamination sensitivity

Sub-visible cirrus cloud is defined by an optical thickness not greater than 0.05. Three optical thicknesses (0.01, 0.02, and 0.05) were investigated. Very thin cirrus with an optical thickness of 0.01 attenuates VIIRS IR measurements by approximately 0.5 K, but with 0.05 optical thickness a brightness temperature depression of up to 2.5 K for some bands is possible. Figure 20 shows the root mean square difference caused by the presence of thin cirrus. The cirrus cloud attenuation is systematic, and the bias can be removed if these sub-visible cirrus clouds can be detected or if a correction is made. Sub-visible cirrus detection and correction prior to PW retrieval can improve PW performance.

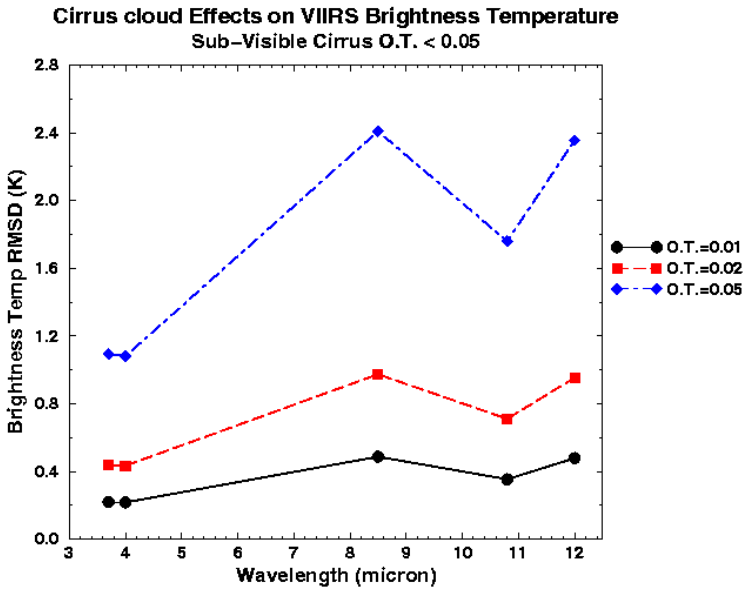

Figure 20. Effects of thin cirrus contamination on TOA brightness temperature in five VIIRS bands.

Figure 21 shows the consequences of thin cirrus contamination, for both no correction and a perfect correction. When the cirrus cloud is very thin, the PW retrievals have very small differences regardless of knowledge of cloud. When sub-visible cirrus grows thicker, the contamination can degrade PW up to 3 to 4 percent.

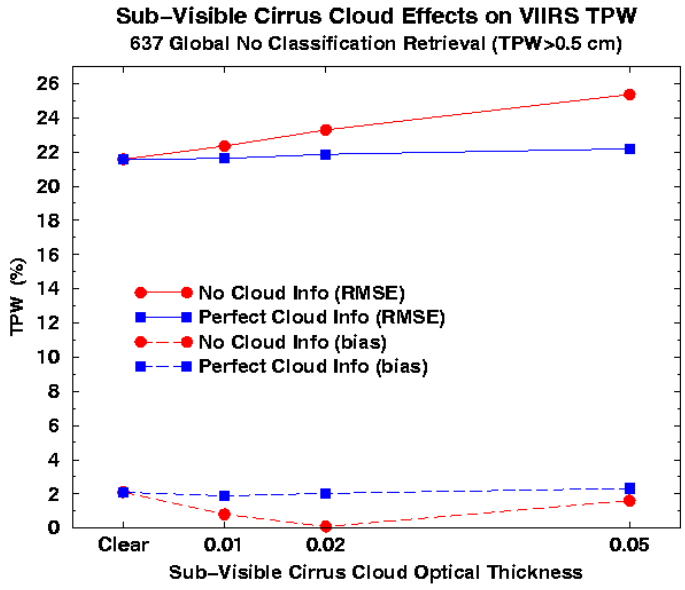

Figure 21. PW uncertainty (RMSE) and accuracy performance due to cirrus contamination. Both uncertainty and bias are given in units of percent of true value.

3.4.1.6 Classification benefits

As described in section 3.4.1, one unclassified and five classified sets of global PW retrieval regression coefficients were derived. In this section, the PW retrieval performance using the unclassified and classified approaches is compared. Figure 22 is the scatter plot of these two approaches. In general, the unclassified approach shows larger scatter than the classified approach for a wide range of PW values. In wintertime (February), the uncertainties of PW retrieval for unclassified and classified are 35.4% (correlation=0.878) and 33.7% (correlation=0.910), respectively. In summertime (month of August) the uncertainties of PW retrieval for unclassified and classified are 29.7% (correlation=0.757) and 25.2% (correlation=0.847), respectively. This result demonstrates that the classified PW retrieval will outperform unclassified for all seasons. The following sections will use only the classified PW retrieval to demonstrate PW sensitivity to other conditions such as, land vs. ocean, night vs. day, and ice vs. water cloud.

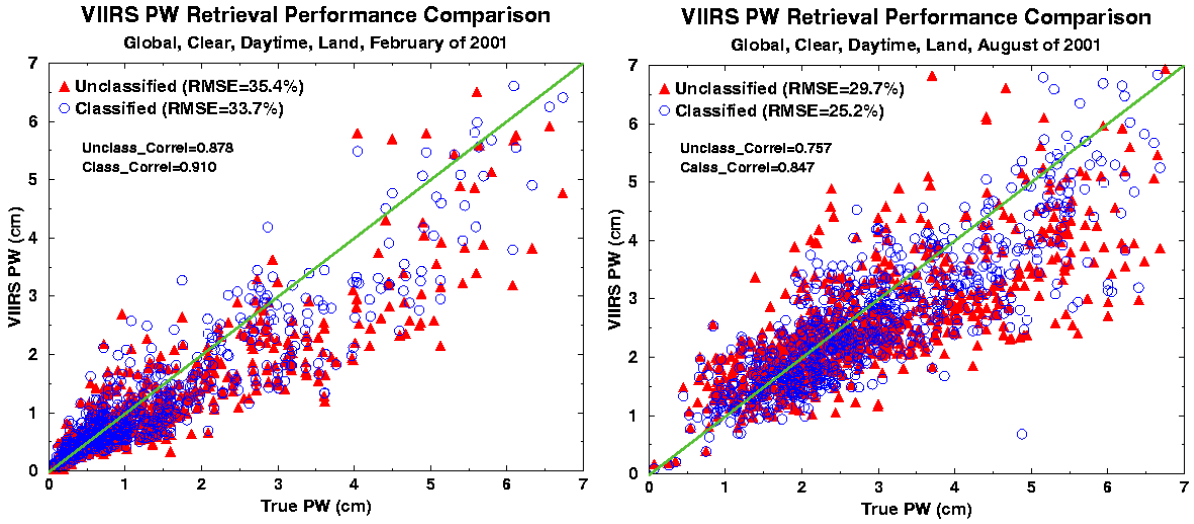

Figure 22. Scatter plot of retrieved versus true PW (left panel – 717 February PW, right panel – 743 August PW); blue open circles are for classified, red closed triangles are for unclassified.

3.4.1.7 PW retrieval sensitivity – Night Vs. Day

Solar zenith angle is used as an independent predictor in VIIRS baseline non-linear retrieval described by equation 28. Figures 16 and 17, which were used to demonstrate the PW EDR uncertainty dependence on surface emissivity, also show that in addition to the major PW information of the infrared signal, the solar component signal can incrementally increase PW EDR performance. Table 5 summarizes the ideal EDR performance improvement due to the

solar signal. In reality, however, the solar component signal may be difficult to model accurately, and a portion of this incremental PW information might be lost.

Table 5. Nighttime vs. daytime PW EDR performance (RMSE).

Case		Day	Night	Difference (Night – Day)
February	Land	33.7%	34.7%	1.0%
	Ocean	30.9%	32.3%	1.4%
August	Land	25.2%	27.1%	1.9%
	Ocean	24.1%	25.3%	1.2%
Note that in summer and over ocean day time PW has best EDR performance				

3.4.1.8 PW retrieval sensitivity – Winter Vs. Summer

As can been from Table 6, using uncertainty of retrieved PW, summertime exhibits lower uncertainty because there is so much more moisture in the atmosphere. The use of PW uncertainty cannot uniquely define PW retrieval skill for different types of atmospheres, since the same PW uncertainty does not imply the same level of absolute PW error.

Table 6. Winter vs. summer PW EDR performance (RMSE).

Case		Winter (Feb., 2001)	Summer (Aug., 2001)	Difference (Winter-Summer)
Day	Land	33.7%	25.2%	8.5%
	Ocean	30.9%	24.1%	6.8%
Night	Land	34.7%	27.1%	7.6%
	Ocean	32.3%	25.3%	7.0%
Note that in summer and over ocean daytime PW has best EDR performance				

3.4.1.9 Cloudy retrievals – Ice and Water Cloud cases

Under cloudy conditions, the PW EDR is defined as the integrated water vapor along the line of sight down to the cloud level only. In this analysis, cloud height knowledge is assumed to have 30 mb uncertainty for ice clouds

and 50 mb for water clouds. Cloud emissivity knowledge derived from COT is assumed to have 10% uncertainty. Retrieved PW uncertainty is shown as a function of ice COTs (0.02, 0.5 and 5.0) and water cloud is assumed to be completely opaque in figures 23 to 26, respectively.

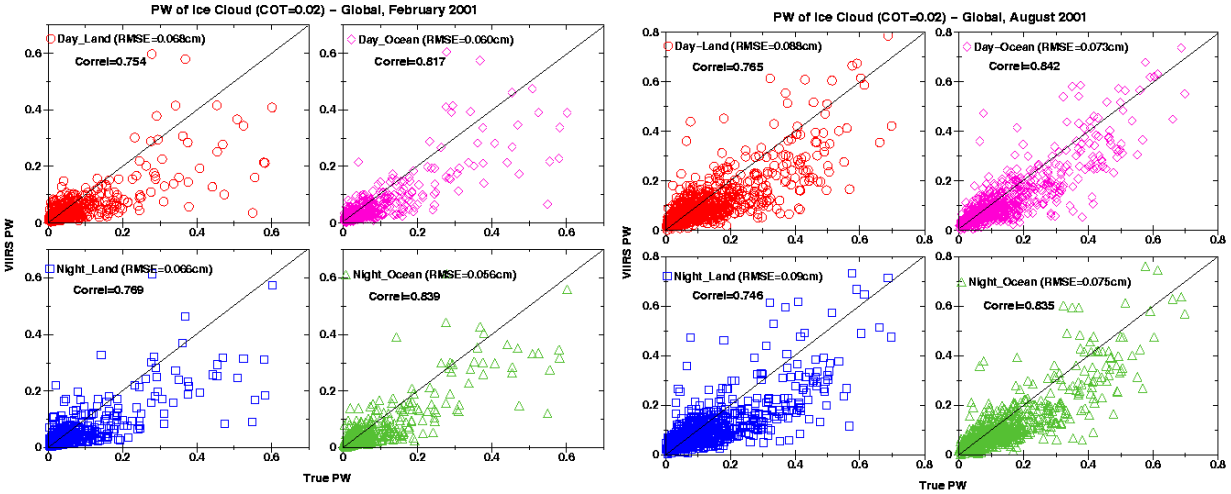

Figure 23. Scatter plot of retrieved versus true ice cloud (at 300 mb and COT=0.02) PW (left panel – 717 February PW, right panel – 743 August PW); four panels of each plot are upper left – daytime over land; upper right – daytime over ocean; lower left – nighttime over land; lower right – nighttime over ocean.

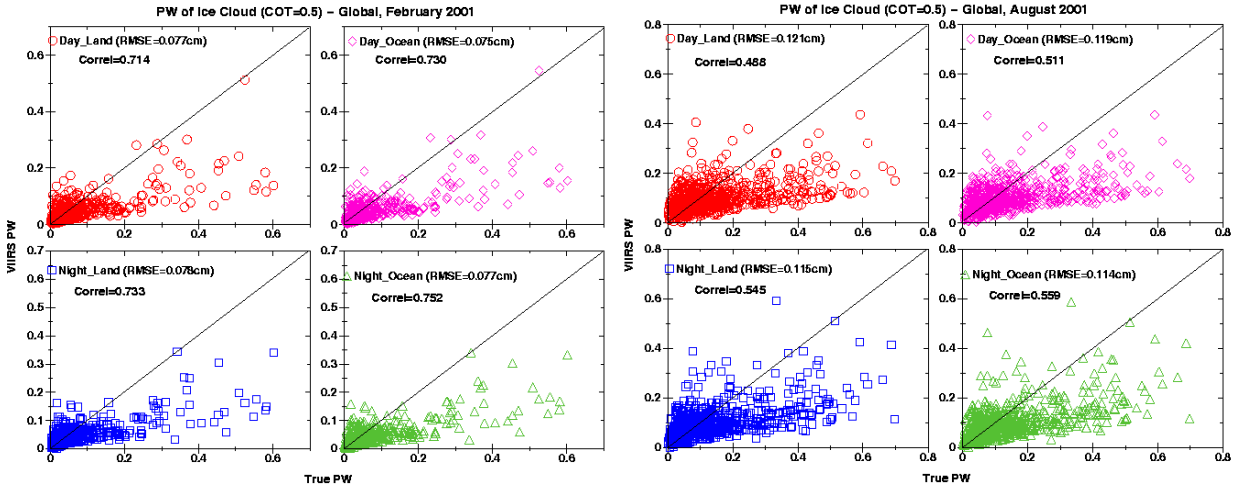

Figure 24. Scatter plot of retrieved versus true ice cloud (at 300 mb and COT=0.5) PW (left panel – 717 February PW, right panel – 743 August PW); four panels of each plot are upper left – daytime over land; upper right – daytime over ocean; lower left – nighttime over land; lower right – nighttime over ocean.

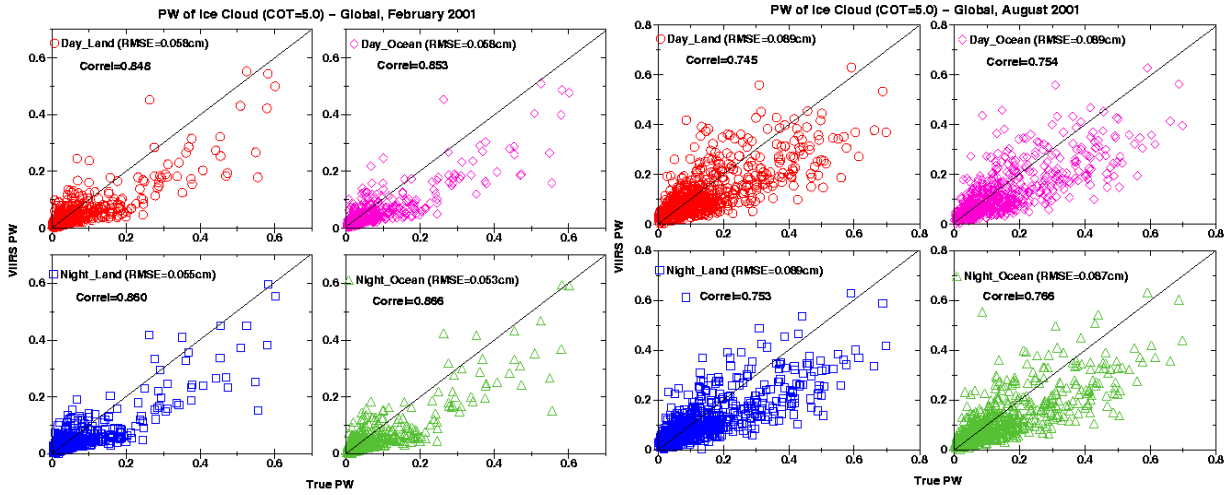

Figure 25. Scatter plot of retrieved versus true ice cloud (at 300 mb and COT=5.0) PW (left panel – 717 February PW, right panel – 743 August PW); four panels of each plot are upper left – daytime over land; upper right – daytime over ocean; lower left – nighttime over land; lower right – nighttime over ocean.

Figure 26 displays water cloud PW EDR retrieval scatter plots for both wintertime and summertime over land, ocean, day and night conditions.

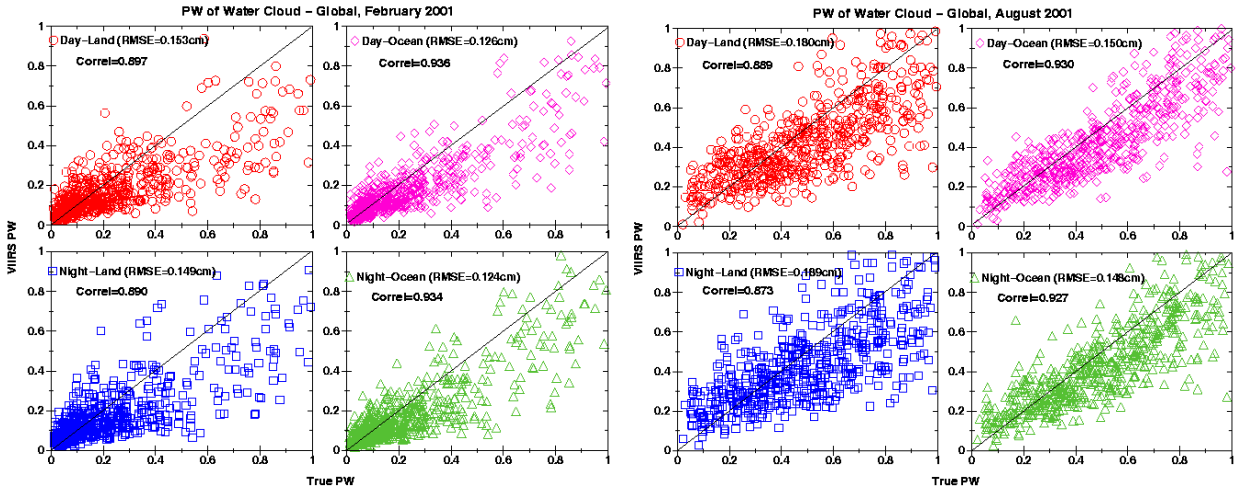

Figure 26. Scatter plot of retrieved versus true opaque water cloud (at 700 mb) PW (left panel – 717 February PW, right panel – 743 August PW); four panels of each plot are upper left – daytime over land; upper right – daytime over ocean; lower left – nighttime over land; lower right – nighttime over ocean.

Table 7 summarizes PW EDR performance in terms of retrieval uncertainty in units of cm. It is shown that at medium COT (0.5), PW has the largest uncertainty. When ice cloud is nearly opaque (COT=5.0) its PW EDR uncertainty is seasonally dependent, but not day vs. night or land vs. ocean dependent. It is also surprising to see that the solar signal is not contributing any significant retrieval information. This might be due in part to inadequate forward modeling of

cloud reflectance in the VIIRS simulation. More detailed study is required to confirm this current analysis.

Table 7. Ice Cloud PW EDR Uncertainty (cm).

Ice Cloud (Cloud Pressure = 300 mb)								
COT	Winter (Feb., 2001)				Summer (Aug., 2001)			
	Land		Ocean		Land		Ocean	
	Day	Night	Day	Night	Day	Night	Day	Night
0.02	0.068	0.066	0.060	0.056	0.088	0.090	0.073	0.075
0.5	0.077	0.078	0.075	0.077	0.120	0.115	0.119	0.114
5.0	0.058	0.055	0.068	0.053	0.089	0.089	0.089	0.087
Numbers shown are PW EDR uncertainty in cm								

Table 8 summarizes water cloud PW EDR performance in terms of its retrieval uncertainty in units of cm. It shows that water cloud PW EDR uncertainty behavior is similar to that for ice cloud, where it is seasonally dependent, only slightly day vs. night or land vs. ocean dependent.

Table 8. Water Cloud PW EDR Uncertainty (cm).

Water Cloud (Cloud Pressure = 700 mb, opaque)								
Winter (Feb., 2001)				Summer (Aug., 2001)			
Land		Ocean		Land		Ocean	
Day	Night	Day	Night	Day	Night	Day	Night
0.153	0.149	0.126	0.124	0.180	0.189	0.150	0.148
Numbers shown are PW EDR uncertainty in cm							

Table 9 displays the computed correlation between retrieved PW and its true PW counterpart as another measure of the potential cloud PW EDR performance. It can be seen that retrieved ice cloud PW exhibits great diversity from a low correlation of 0.488 (ice cloud COT=0.5 in summer under daytime land surface condition) to a high correlation of 0.866 (ice cloud COT=5.0 in winter under nighttime ocean surface condition). Further investigations are needed to address

these disparities. For water clouds, high PW EDR correlation with true PW is indicative of high probability of good performance relative to ice cloud.

Table 9. Ice and water Cloud PW EDR retrieval correlation with true PW (nd).

Ice Cloud (Cloud Pressure = 300 mb); Water Cloud (Cloud pressure = 700 mb)								
Ice Cloud COT	Winter (Feb., 2001)				Summer (Aug., 2001)			
	Land		Ocean		Land		Ocean	
	Day	Night	Day	Night	Day	Night	Day	Night
0.02	0.754	0.769	0.817	0.839	0.765	0.746	0.842	0.835
0.5	0.714	0.733	0.730	0.752	0.488	0.545	0.511	0.559
5.0	0.848	0.860	0.853	0.866	0.745	0.753	0.754	0.766
Water Cloud	0.897	0.890	0.936	0.934	0.889	0.873	0.930	0.927
Numbers shown are correlation between retrieved PW and simulated true PW								

3.5 PRACTICAL CONSIDERATIONS

3.5.1 Numerical Computation Considerations

Paragraph SRDV3.2.1.5.4-1 of the VIIRS SRD states the following:

> "The scientific SDR and EDR algorithms delivered by the VIIRS contractor shall be convertible into operational code that is compatible with a 20 minute maximum processing time at either the DoD Centrals or DoD field terminals for the conversion of all pertinent RDRs into all required EDRs for the site or terminal, including those based wholly or in part on data from other sensor suites."

RDR here stands for Raw Data Record. This essentially means that any and all EDRs must be completely processed from VIIRS raw data, including calibration and geo-referencing within 20 minutes from the time the raw data are available. This requirement is a strong reminder that VIIRS is an operational instrument.

The non-linear PW regression requires little computer time to retrieve PW, but it does require offline computation of classified retrieval coefficient sets. A monthly update of these coefficient sets is expected using 4 months of historical global radiosonde profiles (-13, -12, -11, and -1 month; see section 3.4.1 part 1). Near-real-time surface pressure information is also required.

3.5.2 Programming and Procedural Considerations

The VIIRS baseline PW algorithm is straightforward and easily implemented. Table 10 provides an outline of the procedure for determining PW EDR.

Table 10. PW EDR retrieval procedure.

Step	Description
1	Obtain VIIRS data: radiances, sun-sensor geometry, and cloud mask and cloud phase (ice or water cloud) results.
2	Obtain ancillary data (surface pressure and type) required by algorithms.
3	Classification. Execute VIIRS longwave IR window band classification algorithm.
4A	Clear: Execute non-linear clear PW regression retrieval algorithm. Go to step 5.
4B	Water cloud: Execute non-linear water cloud PW regression retrieval algorithm. Go to step 5.
4C	Non-Water cloud (Ice, mixed, and water/ice): Execute non-linear non-water cloud PW regression retrieval algorithm. Go to step 5.
5	Perform quality checks
6	Store "final" values of PW and quality flags in database for EDR.

3.6 ALGORITHM VALIDATION

Pre-launch field experiment data sets emulating measurements of VIIRS and related in-situ data can provide best validation of the algorithm. Past and scheduled experiments such as CAMEX-II, CAMEX-III, SUCCESS, WINCE, WISC-T2000, SAFARI 2000, as well as Terra-MODIS data, can be used to validate the algorithm by comparing retrieved PW from MAS and MODIS measurements with regular radiosonde and special in-situ PW observations. The required validation data and procedures that can be used for validating algorithm performance can be briefly summarized as:

- Collect statistically significant samples of co-located in-situ PW measurements and VIIRS-like measurements.
- Modify/create VIIRS-like measurements with VIIRS instrument specification noise.
- Perform EDR retrieval using ATBD described algorithms.
- Co-register in-site-measurements and EDR retrievals by taking into account spatial, temporal, and viewing discrepancies.
- Obtain statistical accuracy, precision, and uncertainty estimates of EDR using retrievals and in-situ measurements.

4.0 ASSUMPTIONS AND LIMITATIONS

4.1 ASSUMPTIONS

The following assumptions are made with respect to the retrievals described in this document:

- The fast infrared forward model calculation under cloudy conditions assumes blackbody behavior by the clouds except for ice cloud where input COT defines the non-blackbody cloud effects.
- No rigorous quality checking was applied to PW retrievals, except that PW was not allowed to be negative.
- It is assumed that no sub-pixel clouds exist.
- At this time, mixed phase and multi-layer cloud conditions are not modeled in the radiative transfer calculation. Degraded performance is expected when these clouds are present within the same pixel.
- Schemes for the detection of, and correction for, aerosol and thin cirrus cloud effects are yet to developed and implemented. The next version of this ATBD will reflect progress in this area.

4.2 LIMITATIONS

The following limitations apply to the at-launch retrievals as described in this document:

- Solar reflectivity and emissivity are modeled theoretically, and further validation of the models is needed.
- The fast infrared forward model is also in need of further validation.
- The analyses and results presented in this current version of the ATBD are to a large extent theoretically based. Further extensive validation of the PW EDR retrieval using real VIIRS-like measurements is required.

No major limitations have been identified for the PW retrieval algorithm. It is applicable both day and night, and results indicate that accurate PW EDR retrieval is possible over a wide range of moisture conditions. We do expect degraded performance when mixed phase, multi-layer and sub-pixel clouds are present within a pixel. The impacts of these conditions on PW retrieval accuracy have not yet been quantified.

5.0 REFERENCES

Chesters, D., L. W. Uccellini, and W. D. Robinson, 1983: Low-level water vapor fields from the VISSR Atmospheric Sounder (VAS) "split window" channels. J. *Clim. Appl. Met.*, 22, 725-743.

Hannon, S., L. L. Strow, and W. W. McMillan, 1996: Atmospheric Infrared Fast Transmittance Models: A Comparison of Two Approaches. *Proceedings of SPIE Conference 2830*, Optical Spectroscopic Techniques and Instrumentation for Atmospheric and Space Research II.

IPO (2000). Visible/Infrared Imager/Radiometer Suite (VIIRS) Sensor Requirements Document (SRD) for National Polar-Orbiting Operational Environmental Satellite System (NPOESS) spacecraft and sensors, Rev. 2b/c. Prepared by Assoc. Directorate for Acquisition, NPOESS Integrated Program Office, Silver Spring, MD.

Jedlovec, G. J., 1987: Determination of atmospheric moisture structure from high resolution MAMS radiance data. Ph.D. Thesis, University of Wisconsin-Madison.

Kleespies, T. J., and L. M. McMillin, 1984: Physical retrieval of precipitable water using split window technique. Preprints Conf. On Satellite Meteorology/Remote Sensing and Applications, AMS, Boston, 55-57.

Planet, W.G. (ed.), (1988). Data extraction and calibration of TIROS-N/NOAA radiometers. NOAA Technical Memorandum NESS 107 – Rev. 1, Oct. 1988. 130 pp.